Geophys. J. Int. (2009) **177,** 755–782 doi: 10.1111/j.1365-246X.2009.04077.x

Variations in magmatic processes along the East Greenland volcanic margin

Max Voss, Mechita C. Schmidt-Aursch and Wilfried Jokat

Alfred Wegener Institute for Polar and Marine Research, Columbusstrasse, 27568 *Bremerhaven, Germany. E-mail: Max.Voss@rwe.com*

Accepted 2008 December 9. Received 2008 December 5; in original form 2007 June 30

SUMMARY

Seismic velocities and the associated thicknesses of rifted and igneous crust provide key constraints on the rifting history, the differentiation between non-volcanic and volcanic rifted margins, the driving force of magmatism at volcanic margins, that is, active or passive upwelling and the temperature anomaly in the lithosphere. This paper presents two new wide-angle seismic transects of the East Greenland margin and combines the velocity models with a compilation of 30-wide-angle seismic velocity models from several publications along the entire East Greenland margin. Compiled maps show the depth to basement, depth to Moho, crustal thickness and thickness of high velocity lower crust (HVLC; with velocities above 7.0 km s^{-1}). First, we present two new wide-angle seismic transects, which contribute to the compilation at the northeast Greenland margin and over the oceanic crust between Shannon Island and the Greenland Fracture Zone. Velocity models, produced by ray tracing result in total traveltime rms-misfits of 100–120 milliseconds and χ^2 values of 3.7 and 2.3 for the northern and southern profiles with respect to the data quality and structural complexity. 2-D gravity modelling is used to verify the structural and lithologic constraints. The northernmost profile, AWI-20030200, reveals a magma starved break-up and a rapidly thinning oceanic crust until magnetic anomaly C21 (47.1 Ma). The southern seismic transect, AWI-20030300, exhibits a positive velocity anomaly associated with the Shannon High, and a basin of up to 15 km depth beneath flood basalts between Shannon Island and the continent–ocean boundary. Break-up is associated with minor crustal thickening and a rapidly decreasing thickness of oceanic crust out to anomaly C21. The continental region is proposed to be only sparsely penetrated by volcanism and not underplated by magmatic material at all compared to the vast amount of magmatism further south. Break-up is proposed to have occurred at the seaward boundaries of the continent–ocean transition zones at between ∼50 and ∼54 Ma, propagating from north to south based on a joint analysis incorporating transects from the Kejser Franz Joseph Fjord and Godthåb Gulf. Secondly, the variation of the HVLC along the East Greenland margin from 60° to 77°N and from transects of its conjugate margin shows inverted emplacement of prominent landward and seaward HVLC thickness portions from north to south in a distribution chart. The differences in the HVLC distribution are attributed to one or more of the following three models. In the first model it is inferred that a transfer zone/detachment acts as a barrier to northward magma flow. In the second model, underplating results in thicker and highly intruded lower crust with several small-scale feeder dykes that locally increase the lower crustal velocities. In the third model, a second magmatic event associated with the separation of the Jan Mayen microcontinent is considered. Lithospheric-scale inhomogeneities might be responsible for the heterogeneous melt generation, the inversion of the HVLC distribution in continental and oceanic domains and differences in its velocities.

Key words: Acoustic properties; Continental margins: divergent; Oceanic hotspots and intraplate volcanism; Hotspots; Large igneous provinces; Crustal structure.

1 INTRODUCTION

Many North Atlantic margins are of the volcanic rifted type (White *et al.* 1987; White & McKenzie 1989; Eldholm & Grue 1994). The main characteristics of such margins are (1) seaward dipping reflector sequences (SDRS) (Hinz 1981; Hinz *et al.* 1987), (2) a high velocity lower crust (HVLC) with seismic velocities exceeding 7.0 km s^{-1} (White & McKenzie 1989; Kelemen & Holbrook 1995) and (3) up to three times thicker than normal initial oceanic crust (e.g. Mutter *et al.* 1988; White & McKenzie 1989; Eldholm & Grue 1994). Alternatively, HVLC at non-volcanic margins is attributed to shallow serpentinized mantle rather than melted material (e.g. Whitmarsh *et al.* 1996; Funck *et al.* 2003). Conductive cooling of decompressed melt can explain the exhumation of mantle material and sparsity of magmatism during long-term and pure-shear rifting (Bown & White 1995) at such margins. They have shown that melt thickness increases with lithospheric thicknesses, extension ratios and mantle temperatures, but reduces significantly with the duration of an extensional episode.

SDRS at volcanic margins are generally observed with reflection seismic methods and have been directly sampled by drilling (Eldholm *et al.* 1989; Saunders *et al.* 1998), while the lower crustal structure is inferred from wide-angle seismic (seismic refraction) modelling. Bulk velocities and thicknesses of the crustal layers obtained from seismic *P*-wave velocity models, and the corresponding density models are essential for understanding the formation of volcanic rifted margins (White *et al.* 1987; Mutter *et al.* 1988; White & McKenzie 1989; Bown & White 1995; Kelemen & Holbrook 1995; Korenaga *et al.* 2002). These parameters are effective indicators of the temperatures attained during melt production, and of the melting processes, rift duration and the mantle composition.

New seismic refraction data were acquired in the summer of 2003 (Jokat *et al.* 2004) along four cross-margin profiles between the Jan Mayen and Greenland fracture zones (Fig. 1) in order to assess the temporal and spatial evolution of the northeast Greenland margin. Older seismic lines imaged the structure of the continental crust and sedimentary basins beneath the fjords, and these were extended where appropriate. The aims of the transects are to provide a more detailed image of the continent–ocean transition zone (COT) and the rift-related architecture of the continental crust. The COT, generally well observed at non-volcanic margins, is the region between the thinned continental crust characterized by tilted fault blocks and the onset of oceanic crust marked by magnetic ocean spreading anomalies (Whitmarsh & Miles 1995). Consequently, the continent–ocean boundary (COB) marks the seaward termination of the extended transitional zone. The COB can also be inferred from lateral velocity variations between the continental domain and the newly accreted igneous crust. The COT is commonly less clear at volcanic rifted margins due to the thick wedges of basalts that give rise to seaward dipping reflector sequences, and the large amounts of magmatic intrusions that smear out lateral velocity contrasts. The results of the two southern profiles AWI-20030400 and AWI-20030500 (Fig. 1) reveal a large scale high velocity lower crust and a high degree of magmatic intrusion into the upper crust over a ∼130 km wide continent–ocean transition zone (Voss & Jokat 2007).

The aim of this study is to provide key constraints on the rifting system and timing of continental break-up drawn from the detailed study of the COT, the rift-related crustal architecture, the distribution of magmatic intrusions and flood basalts, and the extent of the HVLC at the northeast Greenland margin. Along-strike variations of the northeast Greenland margin and its crustal architecture will be discussed, and compared with the southern profiles AWI-20030400 and AWI-20030500. A direct line-up of two conjugate transects, AWI-20030300 and a conceptual model of the Lofoten margin, emphasizes their asymmetric structures. The distribution of the HVLC of the East Greenland and the conjugate margins is shown in relation to the mantle plume distance according to an analysis after Barton & White (1995). Three hypothetical models for the formation of the northeast Greenland margin are developed from these observations.

2 BRIEF REVIEW OF GEODYNAMIC MODELS FOR VOLCANIC RIFTED MARGIN

McKenzie & Bickle (1988) and White & McKenzie (1989) inferred the thick basaltic crust at volcanic rifted margins is the result of enhanced melting due to the passive upwelling of mantle material with anomalously high asthenospheric temperatures. A hotspot model developed for the North Atlantic (e.g. Morgan 1971; White *et al.* 1987; White & McKenzie 1989; Skogseid *et al.* 2000) assumes a plume head up to 2000 km wide with a 100–200 °C thermal anomaly, which enhanced decompression melting and increased volcanism during lithospheric extension. Kelemen & Holbrook (1995) deduced major element mantle compositions, that is, the depth of melt generation and migration, from the bulk velocity and thickness of igneous crust. Pure passive upwelling is related to an increased depth range of melt production and higher temperatures, which in turn are associated with higher magnesium and lower silicon contents that are responsible for high average seismic velocities. The formation of the North Atlantic Igneous Province (NAIP) has been associated with the generally accepted model of elevated temperatures from a mantle plume (Iceland hotspot), which has also been hypothesized to have triggered North Atlantic continental break-up (Saunders *et al.* 1997; e.g. White & McKenzie 1989; White 1992). Lawver & Müller (1994) suggested that the mantle plume was located beneath central Greenland in Late Cretaceous/Early Tertiary times (Fig. 1). Thus, the Tertiary volcanism of the North Atlantic margins prior to and during break-up is associated with mantle plume activity within a circle of radius of more than 1200 km.

Systematic seismic investigations along the East Greenland margin over the last 20 yr yield an improved image of its crustal structure (Fig. 1) and have prompted different models of melt generation with or without a mantle plume. The southeast Greenland margin is investigated along four wide angle seismic profiles which show thick igneous crust in the continent–ocean transition zone (COT) and on the first oceanic lithosphere produced after break-up (Korenaga *et al.* 2000; Holbrook *et al.* 2001; Hopper *et al.* 2003). The varying structural styles along the southeast Greenland margin and the presence of the high velocity igneous crust have been linked to their distance from the Iceland plume. Holbrook *et al.* (2001) suggest that a modest margin-wide mantle thermal anomaly was present during break-up (∼56 Ma), which was exhausted by 43 Ma. Active upwelling is proposed for the proximal zone of the plume head, whereas the lateral emplacement of warm plume head material over 500 km (e.g. Sleep 1996) into the distal zone is explained by pure passive upwelling. Active upwelling is understood as the rapid vertical flux of material compared to lithospheric spreading, and may also generate increased seismic velocities of thick igneous crust, but without a thermal anomaly (Kelemen & Holbrook 1995; Holbrook *et al.* 2001; Korenaga *et al.* 2002). Nielsen *et al.* (2002) attribute the

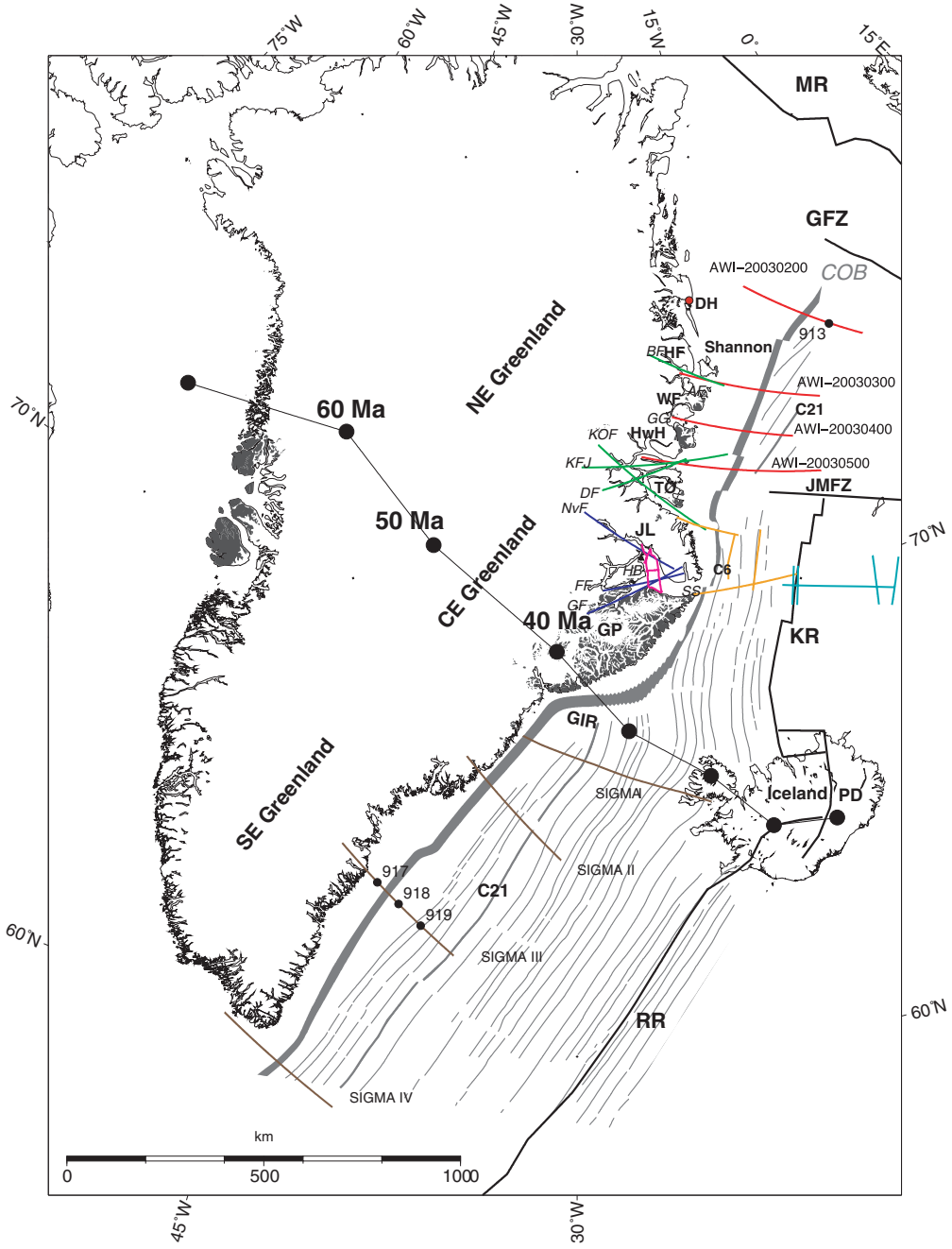

Figure 1. The map of East Greenland shows the margin segmentation into northeast (NE), central-east (CE) and southeast (SE) Greenland. Grey shaded continent ocean boundary (COB), magnetic anomaly lineaments and onshore flood basalts from Escher & Pulvertaft (1995). Magnetic anomalies C21 (marked as thicker grey line) and C6 are labelled. Ridges and fracture zone from Hopper *et al.* (2003). Hotspot track and location proposed by Lawver & Müller (1994). AWI-2003xxxx lines and SIGMA xx lines (see Table 4) are labelled. Colours of seismic lines refer to different sources as described further in the text (Table 4). Small black dots mark ODP sites 9xx. Red dot marks Danmarkshavn (DH). Abbreviations are AF, Ardencaple Fjord; BF, Brede Fjord; DF, Dickson Fjord; FF, Føn Fjord; GF, Gåse Fjord; GFZ, Greenland Fracture Zone; GG, Godthåb Gulf; GIR, Greenland Iceland Ridge; GP, Geikie Plateau; HB, Hall Bredning; HF, Hochstetter Foreland; HwH, Hold with Hope; JL, Jameson Land; JMFZ, Jan Mayen Fracture Zone; KFJ, Kejser Franz Joseph Fjord; KOF, Kong Oscar Fjord; KR, Kolbeinsey Ridge; MR, Mohns Ridge; NvF, Nordvest Fjord; PD, present day location of the Iceland hotspot; RR, Reykjanes Ridge; SS, Scoresby Sund; WF, Wollaston Foreland. Scale is valid for 70° N.

distribution of plume magmatism to the lithospheric base relief in combination with changes in viscosity due to melting. Convective partial melting is proposed to result from lateral thermal gradients in the lithosphere, which passively induce small-scale convection (Mutter *et al.* 1988). Edge-driven small-scale convection cells were proposed to explain the flood basalt provinces at volcanic rifted margins (King & Anderson 1995, 1998). These authors suggest that a step in the lithosphere, for example, at the edge of a thick craton, would control the flow of mantle material into a melting zone, while extension and faulting would allow melt transportation to the surface. Nielsen & Hopper (2004) found that the effect of lithospheric thickness differences was insufficient to produce all

the observed igneous crust at the southeast Greenland margin as a result of edge-effect convection. They propose, instead, that a hot sublithospheric layer is responsible for the temporal evolution of the southeast Greenland igneous crustal thickness. Callot *et al.* (2002) propose a model of localized melting domains, similar to small scale mantle diapirs which arise from the channelled and focused ascent of hot plume material due to such possible edge effects. Such 'soft spots' are invoked to explain the segmentation and along-strike variation of magmatism at the southeast to central-east Greenland margin. Increased mantle temperatures due to the proximal Iceland plume are also assumed for central-east Greenland (Weigel *et al.* 1995; Fechner & Jokat 1996; Schlindwein & Jokat 1999). Alternatives to the mantle plume hypothesis were proposed to explain large scale melt production and mantle temperatures above 1200 °C (McKenzie & Bickle 1988). Anderson (2000) proposed normal potential temperatures for the upper mantle of 1400 ± 200 °C, and rapid convection giving rise to 3-D-heterogenities in the lithosphere that are responsible for the excess magmatism. Foulger & Anderson (2005) considered mantle heterogeneities, resulting from the introduction of subducted slab of oceanic crust beneath the Laurasian continent during the Palaeozoic closure of the Iapetus ocean. Entrainment of subduced crust becomes a major density problem due to phase transformation, which might be solved by sublithospheric convection driven by surface cooling (Korenaga 2004). Other modelling experiments considered mantle upwelling rates that are higher than plate extension rates (van Wijk *et al.* 2001), resulting in the melting of a large amount of normal-temperature mantle material around break-up. Other processes and scenarios were proposed and reviewed for the formation of the North Atlantic Igneous Province by Meyer *et al.* (2007).

The northeast Greenland margin (72° N–78° N) is bounded to the south by the western Jan Mayen Fracture Zone (JMFZ) and by the Greenland Fracture Zone (GFZ) to the north (Henriksen *et al.* 2000). Significant variations in the onshore geology [e.g. the Caledonian orogen, post-Caledonian sediment basins and the distribution of flood basalts (Escher & Pulvertaft 1995; Henriksen *et al.* 2000)], and in offshore features like the width of the shelf region, and magnetic pattern, led to increased interest in the crustal structure of this part of the Greenland margin. Wide aperture CDP profiles and extended spread profiles (ESP) (Hinz *et al.* 1987; Mutter & Zehnder 1988) focused locally on the COT, and the earliest oceanic crust. Seaward dipping reflectors were investigated near the prominent basement structure, the Greenland Escarpment, and the outer high, marking the rise from oceanic crust to the continental slope. This basement structures are similar to the opposing Vøring Plateau Escarpment, which represents the continent ocean boundary and the location of break-up related volcanism (e.g. Hinz *et al.* 1987). Multichannel seismic (MCS) profiles cover the shelf region and parts of the transition from continental to oceanic crust up to ∼73° N (Larsen 1990); Schlindwein & Jokat (1999, 2000) proposed an eastward shift of Mesozoic rifting which preserved the Devonian structures in the region north of Kong Oscar Fjord (Fig. 1) while further thinning and weakening of Devonian crust to the south allowed Tertiary melts to ascend to the surface. Their models did not provide constraints on the COT nor on the onset of oceanic crust. Several seismic and potential field investigations along the opposingM Scandinavian margin provide important constraints on the evolutionary history of the Norwegian–Greenland Sea (Mjelde *et al.* 1997, 1998, 2005; Raum *et al.* 2002; Mjelde *et al.* 2003; Tsikalas *et al.* 2005). Complementary data from the northeast Greenland margin, with comparable coverage and a similar cross-margin extent to those in southeast Greenland, were missing until now. It is debatable therefore, which of the models mentioned above is most applicable to the northeast Greenland margin.

3 NEW TRANSECTS OF THE NORTHEAST GREENLAND MARGIN

The northernmost transect, AWI-20030200, located ∼140 km offshore from Danmarkshavn (Fig. 1), extends across the deep sedimentary basins and shelf slope into the Greenland basin, approximately 200 km south of the Greenland Fracture Zone. Line AWI-20030300 is a prolongation of a previously acquired seismic line 94300 (Schlindwein 1998), and crosses the shelf south of Shannon Island. Profile AWI-20030400 follows the Godthåb Gulf across the shelf, and AWI-20030500 is an extension of the earlier transect 94320 (Schlindwein & Jokat 1999) off the Kejser Franz Joseph Fjord. This contribution presents results for the northern profiles, AWI-20030200 and AWI-20030300.

3.1 Processing and modelling

Data were acquired using the R/V *Polarstern*, with a seismic source array of 77 l (5 × 9L + 32L) (Jokat *et al.* 2004). Ocean bottom hydrophones (OBH) and seismometers (OBS) were deployed offshore and REFTEK stations with geophones were distributed onshore along the Ardencaple Fjord for profile AWI-20030300 (Fig. 2). On both profiles, in-line instrument relocation of 30 to 260 m was performed for those OBH/S that showed asymmetric parabola of the direct wave arrivals in the shot gathers. Bandpass filtering (4–20 Hz) enhanced the data quality for picking arrivals. A projection of the receiver locations from the great circle onto a straight line is obligatory for the ray tracing. A straight line fit through stations 201 and 225 was used for profile AWI-20030200 and revealed a maximum shift of 3.6 km for station 210. The maximum shift, for ocean bottom station 314 on profile AWI-20030300, is 4.3 km for a line through stations 301 and 325 and 14.1 km for the westernmost land station 331 (Fig. 2). The true offsets of the shots and therefore of the observed *P*-wave arrivals, remained unchanged. The contraction of profile AWI-20030300 by a couple of tens of metres within the line, and of approximately 1.2 km within the fjord, due to the projection results in averaging of laterally inhomogeneous crustal structures due to the different ray paths between the real profile and the approximation. However, these errors are expected to have only a minor influence in the overall structural style along the profiles. Individual seismic sections and their ray coverage are shown in Figs 3(a)–(f). In the following we describe the applied modelling methodology for the two transects.

(1) *P*-wave traveltime arrivals were picked with the *ZP* software from *B.C. Zelt* (available at http://www.soest.hawaii.edu/∼bzelt/zp/zp.html). Associated error values for the picks range between 0.04 and 0.15 s and depend on the signal to noise ratio, as calculated by the software in a 0.25 s time window before and after each pick time. A constant error of 0.05 s was used for profile AWI-20030200. First crustal arrivals were weak at stations 202 (Fig. 3c), 210 and 212 of profile AWI-20030200, but could be distinguished better in the first multiples between the station and sea surface.

(2) Velocity models (V_p) were obtained by forward modelling with 2-D ray tracing software *RAYINVR* (Zelt & Smith 1992) equivalent to the procedure applied by Voss & Jokat (2007). 2-D inversion was used in questionable areas of the model but was not the major modelling tool. The error analysis of the individual phases used for the final *P*-wave velocity models are summarized in Tables 1 and 2.

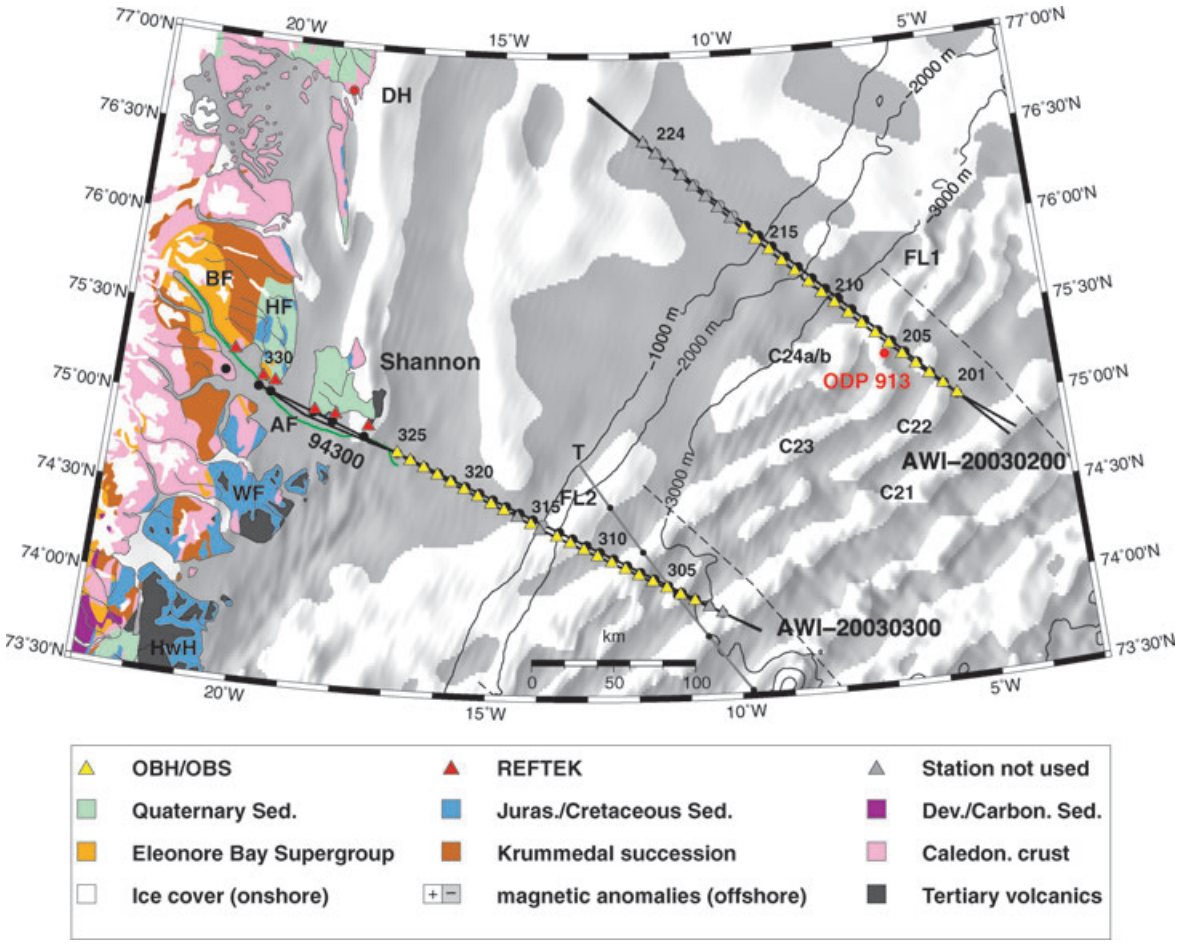

Figure 2. Locations and instruments setup of the seismic refraction profiles AWI-20030200 and AWI-20030300. Background shows regional magnetic grid (Verhoef *et al.* 1996) with white regions for positive and grey regions for negative polarisations. Spreading anomalies are labelled with Cxx. Thin black lines represent bathymetric contours after Jakobsson *et al.* (2000). Onshore geology after Escher & Pulvertaft (1995). Yellow triangles show locations of the OBS/OBH, red triangles represent REFTEK land stations. Black dots show the locations of the receivers projected onto a straight line, as described in the text. Grey triangles and dots mark unused receiver stations. Every fifth station location is labelled. Green line represents seismic refraction profile 94300 of Schlindwein (1998). Dashed thin lines represent synthetic flowlines using the rotation poles of Rowley & Lottes (1988). Thick grey line marks reference transect from Voss & Jokat (2007) with black dots marking picks of spreading anomalies. Abbreviations are as in Fig. 1 and FL1 and FL2, flowlines; T, reference transect. Scale is valid for 75° N.

The phase numbers refer to the layer of the velocity model, for example, P2 means refracted rays in layer 2, and P2P means reflections at the base of layer 2. Reflections at the crust-mantle boundary (Moho) are labelled with PmP, upper mantle refractions with Pn. Occasionally, these refracted waves could not be modelled properly due to the very low vertical gradient of the upper mantle velocities. In these cases the identified arrivals were approximated by a head wave propagating along the Moho and assigned as Pn'. The ray tracing software is able to model multiples at the shot location and the associated phase numbers are labelled with an asterisk. Multiples at the station locations are labelled equally but require manual adjustments prior to ray tracing. A static time shift was applied to the individual picks of the multiples of the above mentioned deep sea stations. The final values are 4.75 s and 4.6 s for the left and right sides of station 202 (3587 m), 4.13 s (left) and 4.16 s (right) for station 210 (3174 m) and 3.1 s for both sides of station 212 (2325 m) depth, which are ±0.1 s of the traveltime path through the water column above the stations. This approximation of the multiples revealed acceptable results, which were used to test the sparse first arrivals of these stations and the layer parameters. Modelling of weak identified arrivals led to large normalized chi-squared (χ^2) values and large RMS misfits between identified and calculated traveltimes. Thus, we spent more effort on fitting the slope of the first arrivals than on minimizing residuals. The remaining deviations between observed and calculated traveltimes should be seen as a best compromise. General resolution tests require equidistant layer and velocity node distributions, which were not appropriate in our models. Thus, the resolution and quality of the final models are obtained from the ray coverage (Figs 4a and 6a) and the fitting parameters. Rays were traced for 97 per cent of 2040 picks (arrivals from the seafloor excluded) for profile AWI-20030200, and 98 per cent of 3550 picks for AWI-20030300 (Figs 4 and 6). A velocity error of ±0.1 km s^{-1} is estimated for the well-covered portions of the oceanic, and the top layer of the continental parts of the profiles. Velocities for the middle and lower continental parts of profile AWI-20030300 (Figs 6 and 7) could not be modelled with errors smaller than ±0.2 km s^{-1}. Layer boundaries were introduced where wide-angle reflections were identified. In all other instances, the layer boundaries were shifted to fit the velocity gradients within the layers. The uncertainties of layer locations were tested by

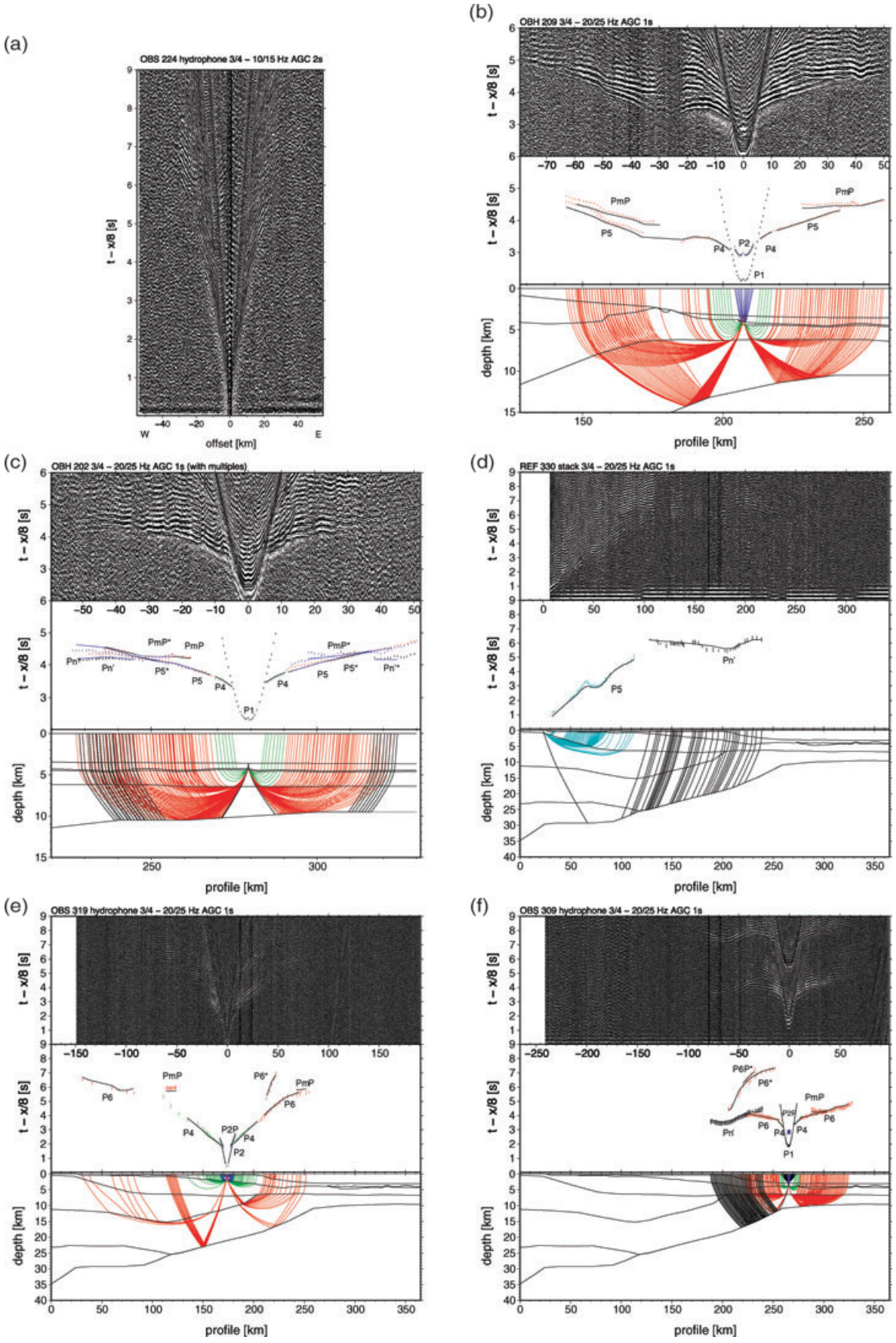

Table 1. Phase nomenclature for individual phases of profile AWI-20030200 with associated number of used observations (n), rms misfit between calculated and picked traveltimes (t_{rms}) in seconds and normalized χ^2.

Layer		Phase	AWI–20030200		
			n	t_{rms}	χ^2
1	Water	Not modelled			
2	top sediments	P2	69	0.055	1.227
		P2P	163	0.186	13.893
3	Oceanic layer 2A	No assigned picks			
4	Oceanic layer 2B	P4	318	0.092	3.413
5	Oceanic layer 3	P5	618	0.081	2.611
		PmP	653	0.091	3.291
	Multiples of oceanic layer 3	PmP*	105	0.073	2.168
6	Mantle (head wave)	Pn'	77	0.078	2.439
	Multiples mantle (head waves)	Pn'*	37	0.057	1.337
	Total		2040	0.097	3.735

Notes: Phases with asterisks are multiples at the receiver locations. Pn' means head waves (details in the text).

Table 2. Phase nomenclature for individual phases of profile AWI-20030300 with associated number of used observations (n), rms misfit between calculated and picked traveltimes (t_{rms}) in seconds and normalized χ^2.

Layer		Phase	AWI–20030300		
			n	t_{rms}	χ^2
1	Water	P1	306	0.149	7.082
2	top sediments	P2	139	0.075	2.034
		P2P	146	0.119	2.065
3	Oceanic layer 2A	No assigned picks			
4	Basalts, continental sediments and	P4	699	0.092	1.778
	Oceanic layer 2B	P4P	33	0.109	1.343
	Multiples of oceanic layer 2B	P4P*	12	0.108	0.914
5	Intermediate continental layer	P5	281	0.130	2.983
		P5P	81	0.123	1.719
6	Lower crust, oceanic layer 3	P6	960	0.093	1.019
		P6P/PmP	431	0.124	1.471
	Multiples of oceanic layer 3	P6*	89	0.100	0.639
		PmP*	21	0.118	0.657
7	Continental sublower crustal layer	PmP	92	0.286	9.577
8	Upper mantle	Pn	61	0.059	0.354
	Upper mantle (head wave)	Pn'	149	0.168	2.340
	Total		3500	0.120	2.265

Note: Phases with asterisk are multiples at the shot point location.

varying the depths until unacceptable misfits occurred for ray tracing. Thus, we estimate the accuracy of layer depths to ±0.1 km for the top reflections (P2P) and the oceanic layers, and ±0.5 km for mid-crustal and Moho reflections.

(3) The final P-wave velocity models were verified by 2-D gravity modelling using commercial software, *LCT*. A predicted gravity model was calculated by converting all velocity nodes of the V_p-models to density nodes using a polynomial formula after Funck *et al.* (2004), which approximates the Nafe–Drake curve (Ludwig *et al.* 1970; Nafe & Drake 1957). Polygons of homogeneous densities were defined within the layer boundaries determined from wide-angle reflections to simplify the initial starting model. A homogenous mantle density (3.31 or 3.26 × 10^3 kg m^{-3}) yields a large error of the modelled gravity. Modifications to crustal layer densities would have only short wavelength effects. The effect of a thickness variation of the lower lithosphere, that is, a higher asthenosphere in the oceanic domain, would result in larger wavelength. An additional influence on density contrasts might be associated with lateral and vertical thermal gradients between the continental and oceanic lithosphere (Breivik *et al.* 1999). Thus, the density for subcontinental upper mantle was set to 3.31 × 10^3 kg m^{-3}, and that for oceanic mantle lithosphere to 3.25–3.26 × 10^3 kg m^{-3} (Figs 5 and 7). Both values should be seen as first order approximations. Equivalent values were used for gravity modelling of the two southern profiles (Voss & Jokat 2007). Densities of the individual polygons were successively modified to fit the short wavelength variations in the measured Bouguer anomalies (Figs 5 and 7). Adjustments within a range of 0.05 × 10^3 kg m^{-3} were necessary. Greater adjustments resulted in large residuals. The depths of layer boundaries within the velocity models were left unchanged.

(4) The geological interpretation of seismic velocities in the continental part of profile AWI-20030300 follows that of velocities in the southern profiles (Voss & Jokat 2007). Detailed lithologic interpretations were not possible due to the lack of boreholes and rock samples. Thus, the velocity models are classified stratigraphically and structurally. Velocities of up to 4.0 km s^{-1} are attributed to post-rift Cenozoic sediments. The velocity variations within this range reflect burial depth and grade of compaction of these sediments. Continental sediments, most likely Mesozoic/ Cretaceous syn-rift sediments, and basaltic extrusive rocks are suggested as the source of P-wave velocities between 4.5 and 6.0 km s^{-1}. P-wave velocities typical for granitic/granodioritic crystalline crust range between 6.0 km s^{-1} at the top and 6.6–6.9 km s^{-1} at the base of the crust (Christensen & Mooney 1995). Velocities greater than this, between 7.0 and 7.4 km s^{-1}, indicate mafic intrusions into the lower crust and/or to mafic underplating between the upper mantle and lower crust (e.g. White & McKenzie 1989). Typical oceanic velocity layering corresponds to sediments (1.6–3.0 km s^{-1}), oceanic layer 2 (4.0–6.5 km s^{-1}) and oceanic layer 3 (6.5–6.9 km s^{-1}) (Fowler 2005). An oceanic layer 3B with velocities of >7.0 km s^{-1} is commonly associated with increased melt production and thickened oceanic crust (White & McKenzie 1989; Eldholm & Grue 1994; Mjelde *et al.* 2001; Tsikalas *et al.* 2005).

(5) Half spreading rates were calculated from regional magnetic data (Verhoef *et al.* 1996) along profiles AWI-20030200 and AWI-20030300 as well as from high resolution aeromagnetic data acquired along the two southern profiles. The results are discussed in a comparison with other calculations of oceanic spreading rates of the East Greenland (Mosar *et al.* 2002b), and the Norwegian Møre margins (Breivik *et al.* 2006).

Figure 3. Examples of recorded seismic data. The traveltime is reduced for 8 km s^{-1}. Observed phases are labelled (see Tables 1 and 2). The ray coverage of each station is marked in the lower model. (a) OBS 224 on profile AWI-20030200, hydrophone channel. A 3–15 Hz band pass filter and automatic gain control window of 2 s is applied. Note the location in Fig. 2 and the scattering of the sediment basin (as deep as 9 s). (b) Station OBH 209 on profile AWI-20030200 shows the loss of signals at the outer high (3–25 Hz and AGC window of 1 s). (c) Station OBH 202 on profile AWI-20030200. Note that phases marked with an asterisk are multiple reflections at the receiver point and shifted statically. Pn' marks arrivals from head waves along the Moho. (d) Land station REF 330 on profile AWI-20030300 shows clearly the Shannon High velocity anomaly. (e) Station OBS 319 on profile AWI-20030300 shows the loss of signals due to the western basin. Note that P6* is a multiple reflection at the shot point. (f) OBS 309 of profile AWI-20030300 is located on oceanic crust. Note the late arrivals of the multiples P6* and P6P* and the head waves Pn'.

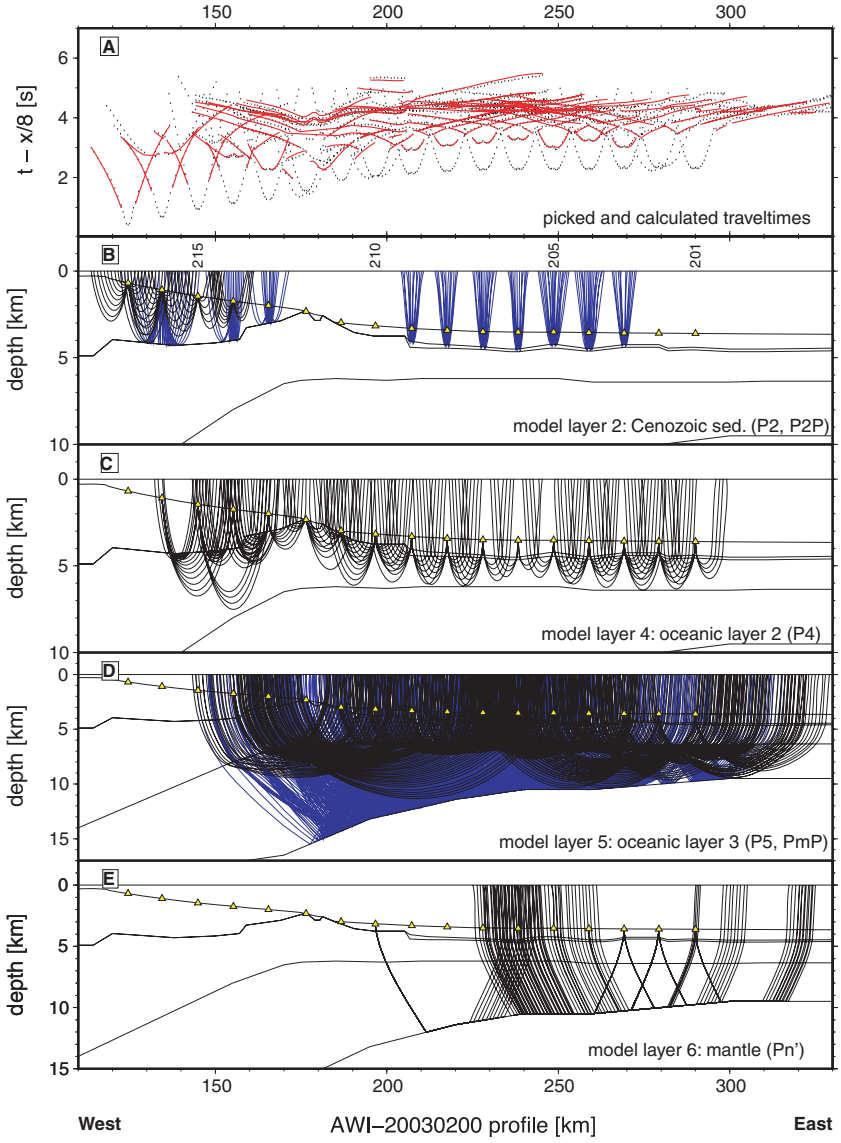

Figure 4. Ray coverage for stations 201–217 along transect AWI-20030200. The first 120 km of the profile were not modelled (see text). (a) Observed and calculated *P*-wave arrivals. The traveltime reduction is 8 km s^{-1}. Picks of arrivals are marked with 50 ms vertical error bar. Red lines show the calculated arrivals (not for picks within the water column). Multiples were modelled for station 202, 210 and 212. (b) Refractions and reflections within the top sedimentary layer. Yellow triangles mark receiver locations were every fifth is labelled. (c) Refractions and reflections of the upper part of the continental basin and oceanic layer 2. (d) As in (c) but for oceanic layer 3. (e) Arrivals interpreted as mantle phases either as refractions or as head waves travelling along the Moho (see text for further explanations).

3.2 Profile AWI-20030200

The 330 km long profile AWI-20030200 runs NW–SE from the continental shelf across a large basement high into the abyssal plain of the Greenland Basin. In total, 25 ocean-bottom hydrophones and seismometers (OBH/S) were deployed (Fig. 2). The eight ocean-bottom stations on the shelf (station 218-225) show a complex pattern of sedimentary phases, as shown in Fig. 3(a) for OBS 224. Most stations recorded no phases from the crystalline crust. This is most probably a consequence of a deep basin and a complex sedimentary structure with low-velocity layers and scattering. The base of the sediments could not be derived from the wide-angle data, or from MCS data (Berger, personal communication). For this reason, only the eastern 210 km of the model, containing parts of the continent–ocean transition and the oceanic layers, will be shown and discussed in this contribution. Fig. 3(b) shows the recording and modelling for OBH 209, which is located near the COB. OBH 202 covers a region of decreasing oceanic crustal thickness and includes modelled multiples, as described above (Fig. 3c). In total, six layers were used: the first layer represents the water, layers 2–5 represent sediments and crustal layering and the sixth layer was used for the upper mantle (Fig. 5).

3.2.1 Continent–ocean transition

Only the eastern part of the COT, including the Greenland Escarpment and an outer high, could be modelled, and the western extent of the transition zone is currently unknown. Near the shelf edge, the sedimentary layer shows seismic velocities between 2.2 km s^{-1} at the top and 3.9 km s^{-1} at 4 km depth (Fig. 5).

The depth to the top basement near the outer high has been constrained by MCS data (Berger, personal communication 2007)

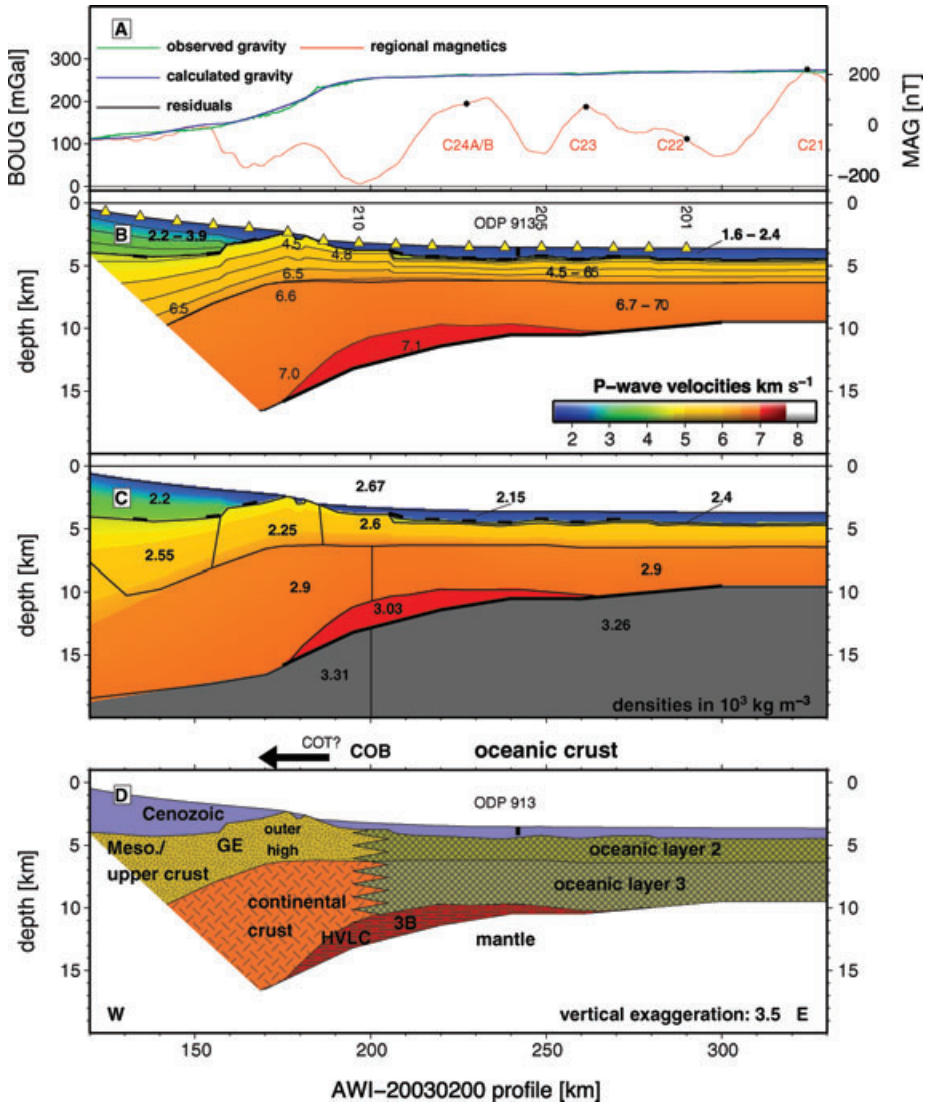

Figure 5. Modelling of profile AWI-20030200. (a) Potential field data along the transect. Magnetic spreading anomalies are labelled. Black dots mark centres of normal polarisation locations for calculations of half spreading rates (see text). Observed and calculated Bouguer gravity and residuals refer to (c). (b) *P*-wave velocity model. Numbers mark velocities of the layers. Contour lines between 2.5 and 7.0 km s^{-1} every 0.5 km s^{-1}. Yellow triangles mark ocean bottom recording locations. Thick black lines outline wide-angle reflections. (c) 2-D density model. Thin black lines mark polygons of constant densities. Colours represent velocity model from (b). The good approximation to the observed gravity is shown by residuals in (a). Note that the splitting of the upper mantle density is a simplification of the thermal effect of suboceanic mantle (see text). (d) Lithologic interpretation based on the models above. The –continent–ocean boundary (COB) marks the seaward end of the transition zone (COT). Abbreviations are GE, Greenland Escarpment; HVLC, high velocity lower crust; Meso., Mesozoic sediments; W/E, west and east.

and by reflections in the wide-angle seismic sections (Figs 4a and b). The crustal structure below the sedimentary layer west of the high (km 120–150) is highly speculative. The Greenland Escarpment, at km 160, and the outer high were modelled with seismic velocities of between 4.5 and 6.5 km s^{-1}. In the lower part of the COT seismic velocities of 6.6–7.1 km s^{-1} were found. Although this area is not well covered by rays (Figs 3b and 4), the modelling results indicate that a large high-velocity body is unlikely.

3.2.2 Oceanic section

The crustal layers have typical velocity ranges for oceanic crust (White *et al.* 1992; Fowler 2005). Deep-sea sediments with a maximum thickness of 1 km were modelled as one layer (1.6–2.4 km s^{-1}). The depth to top basement was derived from MCS data and constrained by reflected phases picked in the wide-angle data (Fig. 4b). The basement topography is quite rough, leading to strong undulations in the crustal phases. Oceanic layer 2A is too small to be resolved by the wide-angle data, but a thin layer (4.3–4.4 km s^{-1}, max. 0.4 km thick) had to be included in order to model the delayed onset of refracted waves from layer 2B. Layer 2B shows seismic velocities between 4.8 km s^{-1} at the top and 6.6 km s^{-1} at the bottom at ∼6 km depth. Velocities of up to 6.7 km s^{-1} were found west of magnetic anomaly C24. In this area, the lower oceanic crustal layer also shows slightly higher velocities (6.8–7.1 km s^{-1}) than towards the end of the profile in the east at anomaly C21 (6.6–7.0 km s^{-1}). The Moho depth decreases from 13 km east of the outer basement high (km 200) to 9.5 km in the deep Greenland Basin (Figs 3b, c and 5). The crustal thickness, without sediments, ranges between 9 km near the transition zone (km 200) and 5 km near C21 (km 300).

3.2.3 Gravity modelling

A simple 2-D density model (Fig. 5) verifies typical oceanic crustal densities with values comparable to other models (e.g. Voss & Jokat 2007). Minimum and maximum deviations of the calculated versus measured Bouguer gravity are in the range of ±11 mGal near the Greenland Escarpment and the outer high (Fig. 5). Further uncertainties result from the unresolved model landward of the outer high. Constraints on the density of the sedimentary layer of the ocean basin were obtained from drilling results. ODP site 913 (Myhre & Thiede 1995), located near km 242 (Fig. 5), yields an average grain-density of 2.5–2.7 $\times$ 10^3 kg m^{-3} and porosities of 30–60 per cent, which would result in densities of 2.2–2.6 $\times$ 10^3 kg m^{-3} for compaction between 0.3 and 0.6 (Sawyer 1985). *P*-wave velocities between 1.6 and 2.4 km s^{-1} are related to densities of 1.65 $\pm$ 0.3 and 2.05 $\pm$ 0.2 $\times$ 10^3 kg m^{-3} (Nafe & Drake 1957). Thus, 2.15 $\times$ 10^3 kg m^{-3} is an acceptable average for the top sedimentary layer. The higher velocities (>7.0 km s^{-1}) in the lower oceanic layer were assigned a slightly higher density of 3.03 $\times$ 10^3 kg m^{-3}, which yield a closer fit of the calculated to the observed gravity. The outer high has densities that are lower than those typical of volcanic structures, which might be attributed to the unresolved model landwards, and/or an unknown internal structure of the outer high. Hinz *et al.* (1987) also found low velocities within the rise seaward of the Greenland Escarpment. A change from 3.31 $\times$ 10^3 to 3.26 $\times$ 10^3 kg m^{-3} marks the transition from subcontinental to suboceanic upper mantle as described above.

3.2.4 Stratigraphic and structural interpretation of AWI-20030200

The oceanic magnetic spreading anomalies provide good constraints on the location of the COB along this transect. Anomalies C24A and C24B form a wide normal polarity anomaly, and can not clearly be distinguished from one another (Fig. 5a). Berger and Jokat (personal communication) confirmed the Greenland Escarpment along MCS lines across the Greenland Fracture Zone, and suggest that basalts were emplaced on continental crust prior to break-up to form the outer high (Fig. 5d). Therefore, we propose the COB to lie at km 200, 20 km east of the outer high within the reversed part of anomaly C24A/B. Seismic velocities of the sediments to the west of this location are significantly higher than the post-break-up sediments east of it. Sediments accumulated landward of the basement high are probably more highly compacted, since they were buried by Palaeogene to Neogene sediments during thermal subsidence (Fig. 5d).

The top oceanic crustal layers, 2A and 2B, are integrated into oceanic layer 2 (Fig. 5d) and can clearly be distinguished from layer 3A based on the velocity structure and density. A high velocity oceanic layer 3B with an initial thickness of up to 2 km terminates near C23. The total thickness of the oceanic crust decreases rapidly seawards, over a distance of 20 km, from 9 to 7 km, near the peak of C24A/B. It decreases to 6 km near the normal polarity part of C23 and further to 5 km near C21. The crustal structure landward of the COB on profile AWI-20030200 contrasts strongly with that derived for the southern profiles AWI-20030400 and AWI-20030500 (Voss & Jokat 2007). This will be discussed further below.

3.3 Profile AWI-20030300

The 365 km long seismic transect AWI-20030300 south of Shannon Island includes 14 OBS, 11 OBH and 6 REFTEK land stations. Stations 301, 302, 314 and 316 (Figs 2 and 6) were not used for modelling due to bad recordings. Phase identification at all other stations was difficult, and could not be improved by filtering. The entire velocity model consists of eight layers; the water column, six layers for sediments and the crust, and one layer for the upper mantle (Figs 6 and 7). Five layers were used to model the continental part of the profile (km 0–210), and four layers for the oceanic part (km 210–365). The westerly 100 km of profile AWI-20030300 overlap with an older seismic profile, 94300, that extends from Shannon Island landwards into the Bredefjord (Schlindwein 1998) and provides additional constraints on the poorly covered (Fig. 6e) and weakly resolved continental crust. The most likely range of the –continent–ocean transition zone and its seaward termination (COB in Fig. 7d) will be discussed further below.

3.3.1 Continental section

The top sedimentary layer, east of Shannon Island, has P-wave velocities of 2.0–2.3 km s^{-1} at the top and up to 3.5 km s^{-1} (km ∼200) at 3 km depth. The sediment thickness increases continuously to 2.7 km (Fig. 7) near km 210. The top of a seaward-necking horizon is constrained by reflections at 1–3 km depth from numerous stations almost continuously between km 145 and 210 (Fig. 6b). The second layer was modelled with velocities, from top to bottom, of between 4.0 and 5.7 km s^{-1}. Wide-angle reflections were inferred from OBS 325, 324 and 320 and constrain the depth of the layer to 6–7 km between km 110 and 160 (Figs 6c and 7). A significant velocity anomaly was found beneath Shannon Island (km 65 and 80). The velocities increase from 4.0 km s^{-1} east and west of the island to 6.0 km s^{-1} beneath it. This positive velocity anomaly is also modelled in layer 5 with a maximum velocity of 6.55 km s^{-1} at 5 km depth and 6.6 km s^{-1} at 13 km depth. Only land stations 331–326 gave constraints on this velocity anomaly (Figs 3d and 6). West of the anomaly, seismic velocities were modelled at between 5.6 and 6.4 km s^{-1} in layer 5 and show a lower velocity gradient than that in the model of the overlapping profile 94300 (Schlindwein 1998). Poor deeper ray coverage by refractions in layer 5 between kilometres 50 and 200 (Fig. 6) results in poor constraints on velocities. Wide angle reflections provide constraints on a likely boundary and help constrain the velocity gradients within the layer (Fig. 6d). It remains questionable, however, if the reflections sampled the same lithological boundary (Fig. 7). Nonetheless, layer 5 velocities range between 5.6–5.8 km s^{-1} at the top and 6.0–6.2 km s^{-1} at the bottom excluding the Shannon Island anomaly (Fig. 7). The base of this layer seems to rise from 15 km to 6.5 km depth between profile kilometres 115 and 190 (Figs 3e and 6d).

The lower part of the crustal model (km 0–120) consists of two layers inferred from profile 94300 in the western overlap (Schlindwein 1998; Figs 2, 6 and 7). Only two very weak reflections (P6P; Fig. 6e) support such a differentiation of the lower crustal layer but no diving waves were observed from the deepest crustal layer between km 0 and 120. The crust-mantle boundary is well imaged by wide-angle reflections and arrivals modelled as head waves, however (Figs 3d and 6f). The range of *P*-wave velocities in these layers of 6.4–7.0 km s^{-1} (top to bottom, kilometres 20–170) and to 8.0 km s^{-1} in the upper mantle (Fig. 7) refers only to the modelling of the head waves. Slightly increased velocities beneath Shannon Island were also necessary to minimize the misfits of PmP reflections (Figs 6 and 7). Large velocity gradient variations towards km 210 necessitated velocities of up to 7.3 km s^{-1} between kilometres 170 and 210 (Figs 3c, d, 6 and 7). A further westward extent of the high velocity lower crustal layer can be precluded from the move out of

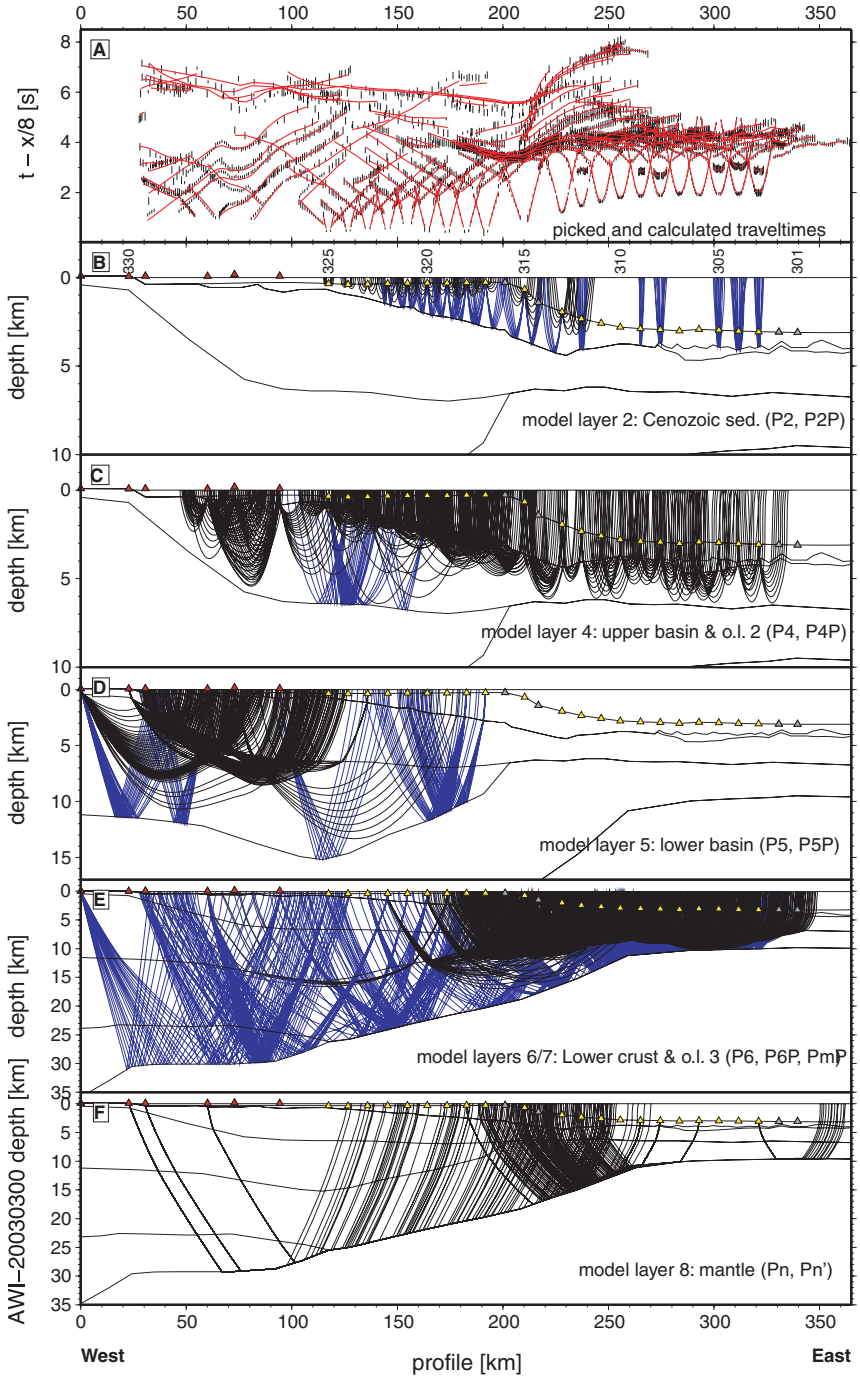

Figure 6. Ray coverage along transect AWI-20030300. (a) Observed and calculated *P*-wave arrivals of all rays. See Fig. 3 for further descriptions. (b) Refractions and reflections within the top sedimentary layer. (c) Refractions and reflections of the upper part of the continental basin and oceanic layer 2. (d) As in (c) but for the lower part of the continental basin. (e) Lower continental crustal rays, oceanic layer 3 and Moho reflections. (f) Arrivals interpreted as mantle phases either as refractions or as head waves travelling along the Moho (see text for further explanations). Abbreviations are o.l., oceanic layer.

the PmP reflections (Fig. 6). Thus, an almost continuous decrease in Moho depth was modelled, from 30 km beneath Shannon Island to 18 km at the onset of oceanic crust.

3.3.2 Oceanic section

The oceanic section between km 210 and 365 (Fig. 7) shows typical seismic velocities, similar to those on profile AWI-20030200 (Figs 5 and 7). The top sedimentary layer (1.6–2.4 km s^{-1}) shows only slightly increased velocities of up to 3.5 km s^{-1} near the COB (km 220). Its thickness varies from 2.7 km to less than 1 km with increasing seafloor depth to 3.1 km. The top oceanic crustal layer is too small to be resolved in wide-angle data, but its existence was derived from MCS data (Berger, personal communication 2007). A thin layer (4.3–4.4 km s^{-1}, max. 0.7 km thick) was added to the model between km 270–365 (Fig. 7) and explains the delay of refractions for the layers beneath. Velocities of 4.3–6.6 km s^{-1} are well resolved in layer 4 from numerous P4 arrivals (Fig. 6).

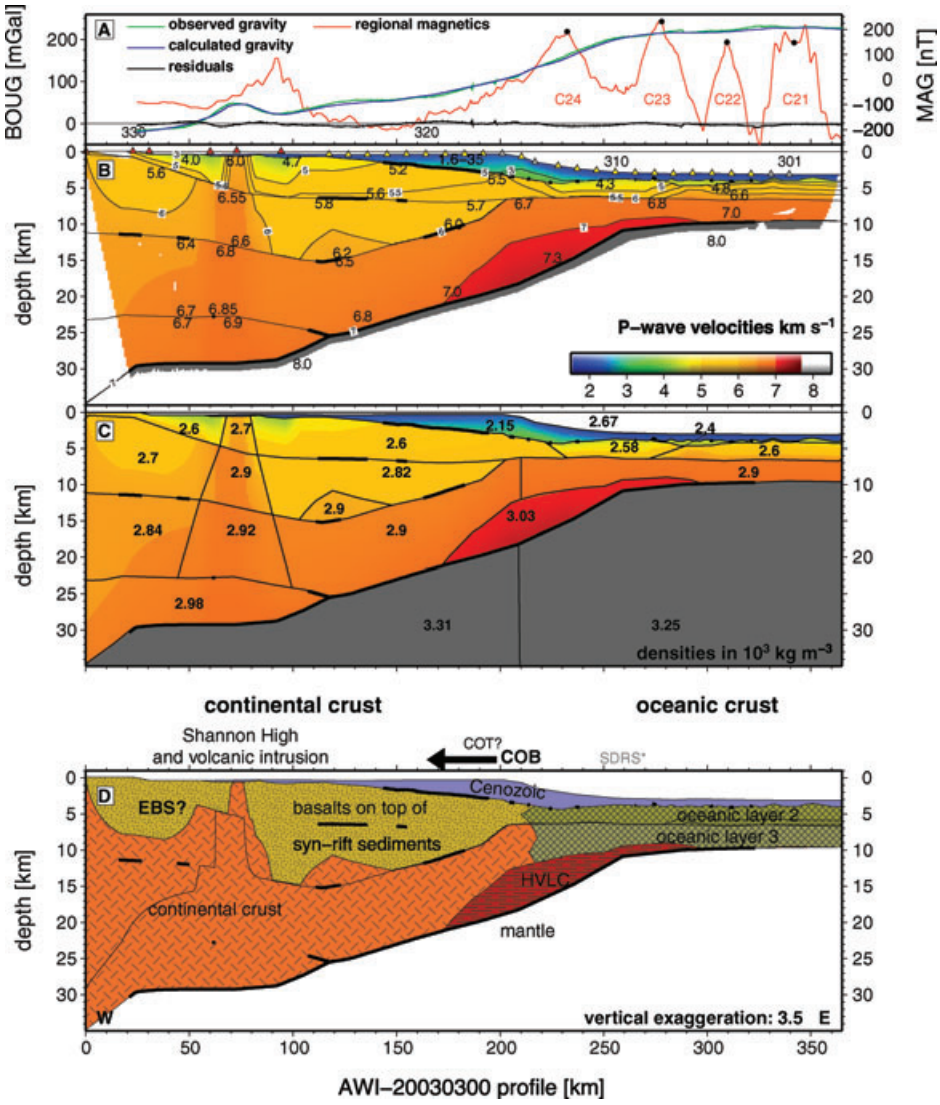

Figure 7. Modelling for profile AWI-20030300. Explanations as in Fig. 5.(a) Potential field data and Bouguer gravity model along the line. (b) *P*-wave velocity model. (c) 2-D density model with marked polygons of constant density. (d) Interpretation of the lithology. Note the likely area for seaward dipping reflectors in the oceanic section between km 220 and 280. Abbreviations are as in Fig. 5 and EBS, Eleonore Bay Supergroup sediments; SDRS*, likely location of seaward dipping reflector sequences.

A significant lower vertical velocity gradient (4.3–5.5 km s^{-1}) was necessary between kilometres 230 and 280 (Figs 3f and 7). The boundary between the two major oceanic layers (model layers 4 and 6) is inferred from the significant change in velocity gradient due to the lack of any P4P reflections (Fig. 6). The lower oceanic layer has velocities of 6.7–7.1 km s^{-1}. Several PmP reflections and Pn arrivals mark the Moho, whose depth increases from 9.5 to 18 km from east to west.

3.3.3 Gravity modelling

The final density model was obtained from the predicted *P*-wave model, as described above, with only minor changes ($\pm 0.1 \times 10^3$ kg m^{-3}) for the density polygons within the continental part (Fig. 7). Minimum and maximum deviations of the calculated to measured Bouguer gravity are in the range of ±8.5 mGal near km 210 and the large Shannon anomaly, respectively. A more significant change for upper mantle densities, similar to that described above, led to the use of densities of 3.31×10^3 kg m^{-3} for the subcontinental and 3.25×10^3 kg m^{-3} for the oceanic upper mantle. The deep velocity anomaly beneath Shannon Island required an introduction of a density anomaly of $0.02–0.2 \times 10^3$ kg m^{-3} higher than the adjacent values. Additionally, a higher lower crustal density (2.98×10^3 kg m^{-3}) beneath the Shannon high was necessary for a satisfactory match to the observed anomalies. Slightly increased velocities (~6.2 km s^{-1}) in 10–13 km depth at km 120 correlate with a gravity anomaly. This anomaly might suggest that the velocities are probably underestimated within the range of uncertainties in this poorly covered region (Fig. 6). The density model verifies the inferred continental crustal velocity model and provides additional constraints for the crustal structure and depth to Moho.

3.3.4 Stratigraphic and structural interpretation of AWI-20030300

The top layer, from the shelf into the ocean basin, is related to post-rift Cenozoic sedimentation. The velocities and density model west of Shannon Island (kilometres 0–50) suggest that a thick pile of Neoproterozoic Eleonore Bay Supergroup (EBS) sediments are concealed beneath Cretaceous sediments, which were deposited between the fjord and Shannon Island (Fig. 7d). The onshore

geology shows EBS sediments along the Brede and Ardencaple Fjord (Fig. 2). Outcrops on Hochstetter Foreland and Shannon Island indicate the presence of Cretaceous sediments beneath Quaternary sediments (Escher & Pulvertaft 1995; Fig. 2). Constraints on the thickness of the EBS sediments can be drawn from the interpretation of profile 94300 (Schlindwein 1998), where velocities of between 5.6 and 6.0 km s^{-1} indicate a pile of sediments 4 km thick. Applying an equivalent interpretation of the velocities, EBS sediments west of Shannon Island would be up to twice as thick (8 km) if the 6.0 km s^{-1} contour line is the deepest limit (Fig. 7).

The two units beneath the Cenozoic sediments east of Shannon Island (km 90–200) are interpreted to represent a deep rift-basin (up to 15 km) with a low vertical velocity gradient. The thickness of basalts erupted close to break-up cannot be resolved. We also assume that the basin east of Shannon Island has a more complex structure with horsts and grabens and probably minor volcanic intrusions at greater depths than can be resolved by the velocity model, which is rather uniform. Scattering, and probably absorption of seismic energy prevents sufficient ray coverage in this part of the profile, and does not allow identifying such structures in detail. Large t_{rms} and χ^2 values (Table 2) for arrivals of model layer 4 leave the exact depth of this likely Palaeozoic/Mesozoic basin debatable (Fig. 7). We interpret the velocity variations and densities between km 90 and 210 as an average taken over this faulted rift zone. The slightly higher velocity and density at 11–15 km depth (kilometre 120) suggest another structural high that is buried deeper in the basin. The sedimentary cover yields a weaker Bouguer anomaly and there is no magnetic anomaly associated with the structural high. Such a deep basin can also be inferred from the regionally low magnetic field anomalies (Fig. 7a) between kilometres 100 and 200. The short wavelength anomalies suggest shallow sources, which can most likely be attributed to flood basalts. This interpretation is consistent with other findings: Larsen (1990) suggested coast-parallel basins and highs across the shelf from aeromagnetic data; Hamann *et al.* (2005) inferred from MCS reflection data that deep basins (<13 km) offshore Shannon Island contain rock successions of Devonian to recent age. These deep sedimentary basins along East Greenland developed during a Devonian phase of extensional collapse (Surlyk 1990). Presumably Mesozoic deposits buried the Devonian strata during uniform extension and subsidence of the basin, equivalent to the situation in the Jameson Land basin. We assume that the Shannon basement high (Fig. 7, kilometres 50–90) also served as a magma conduit inferred from magnetic data and widespread extrusive rocks like those seen in outcrops on Shannon Island. Plateau basalts of Tertiary age with inter-basaltic sediments crop out on Shannon Island and have been related to the Lower Plateau Lava Series, that is, ∼56 Ma (Watt 1994), although no correlation with other flows on Wollaston Foreland was possible (Fig. 2). The positive magnetic anomaly is, however, consistent with volcanism during the normal polarity part of chron C25 (55.9–56.4 Ma; Cande & Kent 1995). The strong reflections between the Cenozoic and older sediments (Fig. 6b) are attributed to a cover with a layer of flood basalts but with an unresolved thickness.

Crystalline basement of continental crust is inferred from velocities greater than 6.0 km s^{-1}. Its thickness decreases significantly from west to east, from nearly 25 km (km 60) just west of the Shannon high to less than 11 km at km 210. Reflection arrivals were modelled at only one station (REF 326) at 23 km depth near profile km 60. This lower crustal reflector is not a significant velocity contrast but is consistent with the model of profile 94300 (Schlindwein 1998). A lithological difference can only be assumed from the gravity modelling. The increased density, and the occurrence of basalts on Shannon Island, supports the existence of a higher degree of magmatic intrusion in the lower crust. As inferred for the profiles off Godthåb Gulf and Kejser Franz Joseph Fjord (Voss & Jokat 2007), there is no evidence of magmatic underplating, as velocities do not exceed 7.0 km s^{-1}, and densities are lower than 3.0×10^3 kg m^{-3}. However, we suggest magmatic intrusions do occur in the lower crust between kilometres 170 and 210, where the increased seismic velocities and the density of 3.03×10^3 kg m^{-3} differ significantly from those of the adjacent continental and oceanic crust (Fig. 7d). The maximum thickness of this high velocity layer (HVLC) is 6 km at km 206, and it terminates into oceanic layer 3 within the oceanic crust. The dimensions, seismic velocities, and density of the high velocity lower crustal part differ significantly from those on the southern profiles, but show similarities to the results from profile AWI-20030200. We therefore assume that the region between profiles AWI-20030300 and AWI-20030200 contains no magmatic underplating at all and that less magmatism accompanied the continental break-up in this part than further south.

A distinct continent–ocean transition zone cannot be defined due to the weakly resolved structure of the basin between Shannon Island and the oceanic crust. The first magnetic anomaly seems to correspond to C24A/B and therefore constrains the eastward limit of the COT. We propose the onset of oceanic crust and, with it, the location of the seaward COB at km 210, which is well constrained by the oldest magnetic spreading anomaly, the density model for the upper mantle and the evidence for magmatic intrusion of the lower crust. The top oceanic crustal layers 2A and 2B are integrated into oceanic layer 2 (Fig. 7d), and can clearly be distinguished from oceanic layer 3 on the basis of their velocities, gradients and density (Fig. 7d). An interface between the continental sediment-basalt mixture and oceanic layer 2 (km 210 and 280) might contain an outer section of SDRS deduced from the slightly reduced velocities and densities (Figs 7b and c). However, in such a position these basaltic wedges would obviously overlay oceanic crust. The total oceanic crustal thickness decreases from 13 km at the COB (km 210) to only 7 km near C23 (km 260) within only 40 km and to only 5.5 km at the end of the profile near C21; a value that is thinner than normal oceanic crust (White *et al.* 1992).

3.4 Comparison of structural style with the conjugate Lofoten-Verstålen margin

The region between Shannon Island and the Greenland Fracture Zone is conjugate to the Lofoten-Verstålen Margin off Norway. Comparable margin transects are selected by constructing synthetic flowlines from the Mohns Ridge to the margins (Fig. 8a), using the rotation poles of Rowley & Lottes (1988). Based on these, two transects, T1 and T4, are suitable for structural style comparisons. Structural interpretations of the Norwegian transects are based on seismic refraction and magnetic/gravity modelling (Kodaira *et al.* 1995; Tsikalas *et al.* 2002; Tsikalas *et al.* 2005); Voss & Jokat (2007) compared profile AWI-20030400 and the Vøring Plateau profile OBS-99 (Mjelde *et al.* 2005), based on a similar reconstruction.

AWI-20030200 is conjugate to transect T4 off the Verstålen margin segment (Fig. 8a), where no HVLC is observed (Tsikalas *et al.* 2005). Normal oceanic crust (∼8 km) is up to 3 km thicker than on line AWI-20030200 (Fig. 8b). The COBs mark the landward increase in Moho depths, which seems shallowly dipping on both margins. The structural styles differ further landward. A marginal outer high bounded by the landward escarpment, as seen on line AWI-20030200 (Figs 5 and 8b), is absent on the conjugate margin.

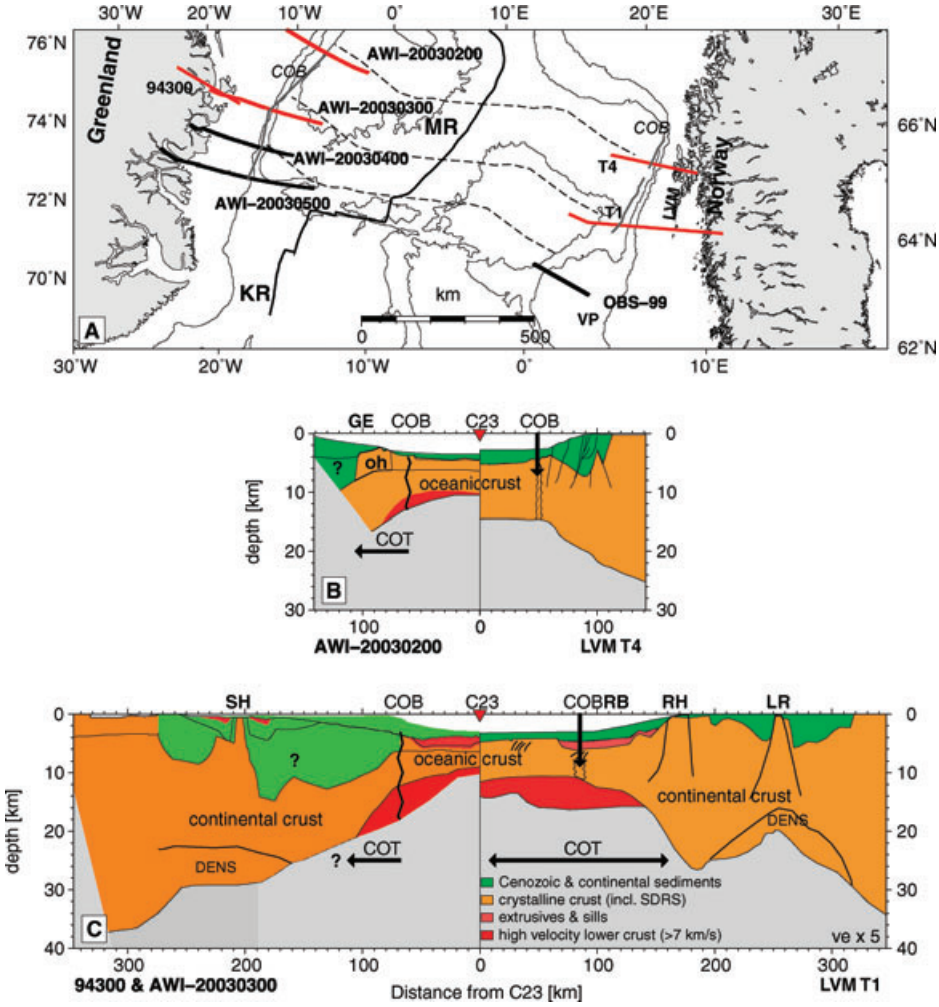

Figure 8. Comparison of profiles from northeast Greenland and Lofoten-Vesterålen Margin (LVM). (a) Line location map. Thick lines mark seismic profiles. Red lines are compared below. Dashed thin lines represent flowlines (Fig. 2) from the Mohns Ridge (MR). Grey lines mark proposed COBs. Thin black lines are bathymetric contours of 1000, 2000 and 3000 m. See text for line references. Abbreviations are KR: Kolbeinsey Ridge, VP: Vøring Plateau. Scale valid for 75° N. (b) + (c) Line-up of simplified conceptual models at chron C23. LVM T1 and T4 after Tsikalas *et al.* (2005). Note that profile lengths are inverted to distance from C23. Hatched lines mark SDRS. Black lines outline structural features. Abbreviations are COB/COT: continent–ocean boundary and transition zone, GE: Greenland Escarpment, DENS: marked lower crustal region with proposed increased density, oh: outer high, LR: Lofoten Ridge, RB: Rørst Basin, RH: Røst High, SDRS: Seaward dipping reflector sequences, SH: Shannon High.

Although no crustal structure is modelled along the East Greenland line west of the escarpment, the general basin style is not symmetric to the conjugate Versterålen margin (e.g. Tsikalas *et al.* 2001; Hamann *et al.* 2005).

A simplified model of transect T1 after Tsikalas *et al.* (2005) is aligned with a simplified structural model of the conjugate profiles 94300 and AWI-20030300 (Fig. 9) at anomaly C23 (Fig. 8c). The major difference is the clear core complex structure at the Lofoten margin segment. There are also clear differences in the widths and depths of sedimentary basins, and Moho depth. The oceanic crust is also approximately 2 km thicker near C23 on the eastern margin. The definition of the COT of the Lofoten margin differs in that it includes the area between C23 and the COB (Fig. 8c), although both COBs are located near the reverse polarity part of the earliest magnetic spreading anomaly (Tsikalas *et al.* 2002; this paper), that is, 70–80 km landward of C23 and seaward of extremely thinned continental crust. The lens-shaped HVLC extends on both transects from C23 into the continental domain and is thickest near the COB. The depth range differs beyond the COB, which correlates with the steady increase of Moho depth on the Greenland side. On the Norwegian side, the HVLC to the south is absent further north (Tsikalas *et al.* 2005), similar to what we suggest for the Greenland side, despite the slightly higher velocities beneath the COB on line AWI-20030200. An adjacent basaltic basin cover is also suggested off Shannon Island but its thickness is not resolved. Seaward dipping reflectors are proposed for both margin segments between the COB and C23, although they are weakly constrained. Continental crust is thinnest between the COB and the Røst High, which is located approximately 75 km eastwards. An equivalent (albeit more deeply buried) high is suggested on line AWI-20030300, ~90 km landward of the COB (Fig. 8b), where continental crust is also thinnest. Both highs are marked by gravity anomalies, although the east Greenland anomaly is weaker and lacks a corresponding magnetic anomaly (Fig. 7a). Further landwards, the Shannon High shows strong similarities to the Lofoten Ridge. Both are distinct highs with proposed increased lower crustal density anomalies. The thinnest crust beneath the Lofoten Ridge is attributed to core-complex development during large scale Mesozoic extension (Tsikalas *et al.* 2005). High grade, lower crustal rocks, and magmatic intrusions at shallow levels are the likely sources of the higher

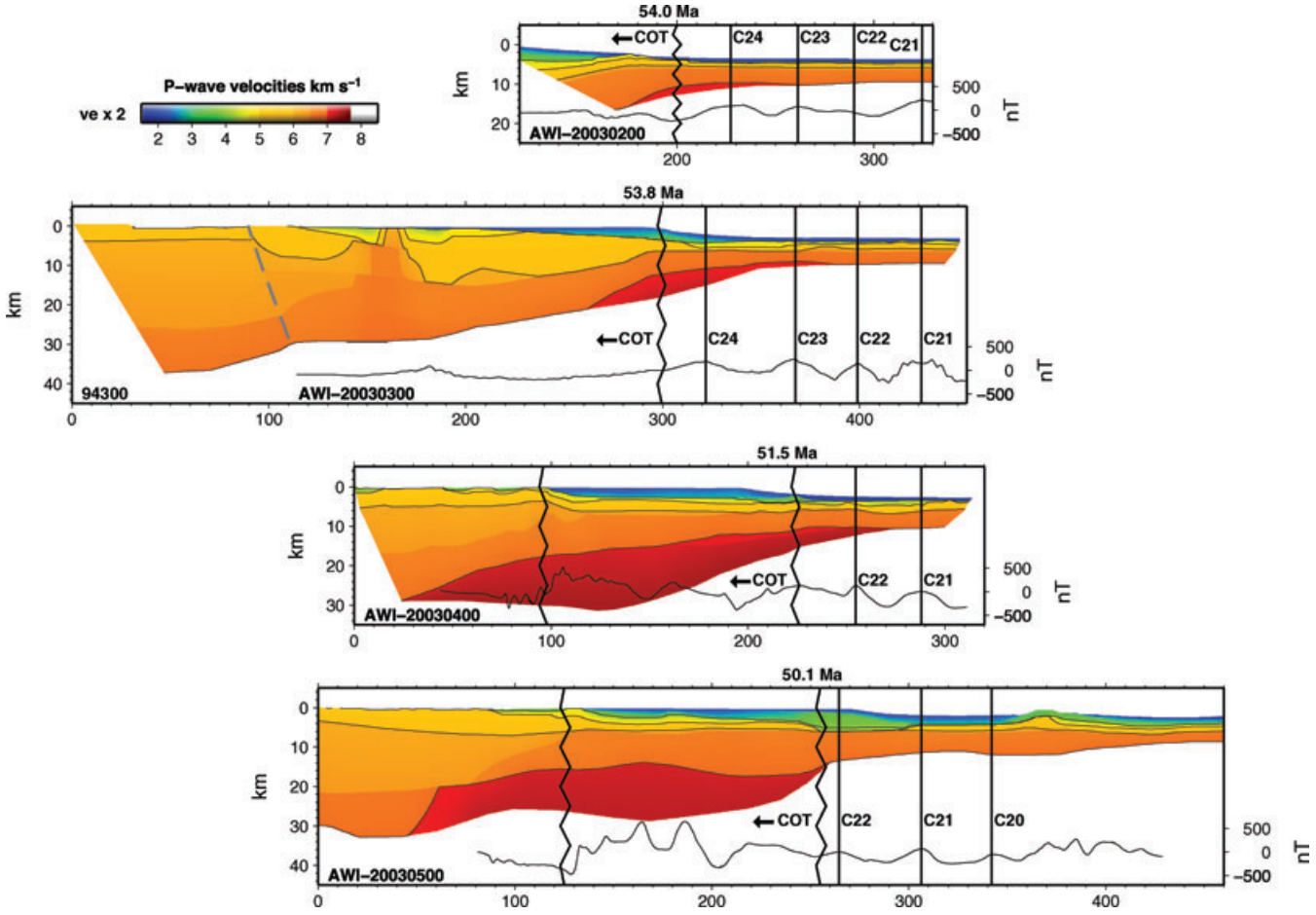

Figure 9. Compilation of northeast Greenland *P*-wave velocity models between the Jan Mayen and Greenland fracture zones. Locations are in Fig. 1. All models are shown with vertical exaggeration of 2 and velocity contours of 4, 5, 6 and 7 km s^{-1}. Model for 94300 refers to Schlindwein (1998), models of AWI-20030400 and AWI-20030500 to Voss & Jokat (2007). Boundary of merged profiles 94300 and AWI-20030300 is outlined with grey dashed line. Lower right scale relates to along-line magnetic data as shown at the bottom of the models. Spreading anomalies and seaward COB of the transition zones are marked with vertical lines and labelled. The age given above the COB refers to calculated time of break-up (see text).

density. The East Greenland margin shows no core-complex structure but magmatic intrusions are proposed consistent with the emplacement of flood basalts on Shannon Island. Thus, volcanism can not be excluded, but the age of this and its possible relationship to Late Cretaceous/Early Palaeocene rifting remains a subject for debate.

The variable oceanic Moho depths, crustal thicknesses, definitions of the COT and the absence of a core-complex emphasize the general asymmetry of these conjugate margins. The outlined small-scale similarities in structural styles and interpretations permit the assumption, however, of a more symmetrical conjugate margin pair than the Vøring and East Greenland margins (Voss & Jokat 2007).

4 HALF SPREADING RATES AND TIME OF BREAK-UP

Voss & Jokat (2007) proposed a north to south rift propagation during opening of the Greenland Basin north of the Jan Mayen Fracture Zone. This proposal is based on the obliquity of the continent–ocean transition zone deduced from crustal structure models of profiles AWI-20030400 and AWI-20030500 with respect to the oldest magnetic spreading anomalies. The new constraints on the seaward terminations of the continent–ocean transition zone developed here (Fig. 9) allow us to determine the time of break-up (Table 3) along the northeast Greenland margin. Minimum and maximum estimates of the timing were derived from calculations of half spreading rates along the profiles, and also by using the average of the half rates over all four profiles, as shown in Fig. 9.

A major difficulty in this is to distinguish between ocean spreading anomalies C24A and C24B along the transects AWI-20030200 and AWI-20030300. On both profiles, only one distinct maximum can be seen that relates to these spreading anomalies (Figs 5a, 7a and 9). Therefore, we average over the time period after Cande & Kent (1995) and estimate a C24 normal polarisation maximum at 52.9 Ma. A similar approach for anomalies C20–C23 results in normal polarisation maxima at 43.16, 47.09, 49.36 and 51.4 Ma. The differences between these age maxima were used for the durations of the spreading intervals. Half spreading rates were determined for C20–C24 along the profiles and corrected for spreading direction (Table 3), based on synthetic flowlines from the Mohns Ridge generated using the rotation poles of Rowley & Lottes (1988). A change in spreading direction occurred after C22. The main uncertainty is in the identification of the peaks of normal polarity anomalies (Figs 5a and 7a), with 2 km shifts yielding an error of 1.5 km Ma^{-1} in the modelled half spreading rate. An offset in magnetic anomaly

Table 3. Half spreading rates and timing of break-up calculated four northeastern seismic lines.

h.s.r. in kmMa^{-1} on profile location	C20–C21 (3.93 Ma)	C21–C22 (2.27 Ma)	C22–C23 (2.04 Ma)	C23–C24 (1.5 Ma)	Break-up at seaward boundary of COT (Ma)
AWI-20030200	–	14.8 (11°)	14.0 (5°)	22.6 (5°)	54.0 ± 0.2
AWI-20030300	–	13.1 (23°)	14.9 (16.5°)	29.0 (16.5°)	53.8 ± 0.2
AWI-20030400	–	13.4 (24.5°)	13.2 (18°)	–	51.5 ± 0.2
AWI-20030500	8.1 (27.5°)	17.1 (27.5°)	−(22°)*	–	50.0 ± 0.3

Note: Angles behind half spreading rates were used to correct for spreading directions. Angle with asterisk was used for break-up calculation.

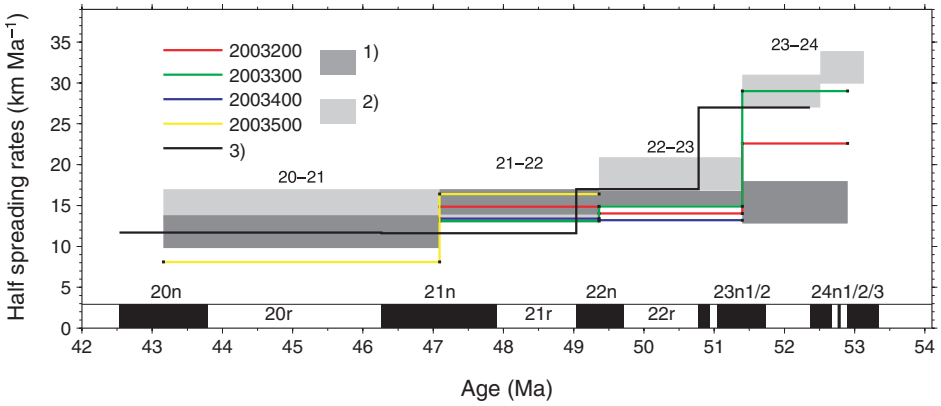

Figure 10. Half spreading rates calculated along seismic lines. Calculations by other authors are included as reference. Dark grey (1) refers to Mosar *et al.* (2002b), light grey (2) to Breivik *et al.* (2006). The half spreading rates of Voss & Jokat (2007) (3) are based on the beginning of each positive polarity anomaly while all others used the maxima of normal polarities. Polarities of the magnetic chrons are shown at the base of the diagram after Cande & Kent (1995).

C22 near stations OBS 201 and 202 on profile AWI-20030200 (Fig. 2) appears on the regional magnetic grid. Here, we have used a projection of the linear part of the anomaly from further southwest. Similar calculations on the southern profiles AWI-2003400 and AWI-20030500 constrain the half spreading rates for the intervals between C21–C23 and C20–22, respectively (Table 3).

For the northern lines, early seafloor half spreading rates range between 22 and 29 km Ma^{-1} (Fig. 10). Later on, rates dropped to 13–15 km Ma^{-1} (average 14 km Ma^{-1}) between C23 (51.4 Ma) and C22 (49.4 Ma) and to 13–17 km Ma^{-1} (average 14.7 km Ma^{-1}) for the interval C22 to C21 (47.1 Ma). A further drop at C21–C20 (43.2 Ma) to below 10 km Ma^{-1}, was determined along line AWI-20030500. These values closely fit published half rates for the intervals between C21 and C23 (Fig. 10). Half spreading rates determined along a transect perpendicular to the magnetic anomalies (Voss & Jokat 2007; Fig. 2), however, judging from the old edges of normal polarity anomalies giving rise to an apparent shift in the determined age of rate changes (Fig. 10).

Mosar *et al.* (2002b) calculated half spreading rates along tectonic flowlines and found much slower rates than we have for the interval between C23 and C24, but identical rates for later intervals. Results from the Møre margin (Breivik *et al.* 2006) also resemble our results quite well. Hopper *et al.* (2003) determined initial half spreading rates of 33 km Ma^{-1} for the southeast Greenland margin between 56 and ∼53 Ma, with a drop to 19 km Ma^{-1} between ∼53 and 50.8 Ma and a further decrease to 17 km Ma^{-1} until 47.8 Ma according to results from Leg 152 (Larsen *et al.* 1994). These rates are comparable to the observations of northeast Greenland, despite the fact that break-up is proposed to be earlier (∼56 Ma).

Based on our half rate calculations, we propose a time of break-up (Table 3) of 54 ± 0.2 Ma at profile AWI-20030200 and 53.8 ± 0.2 at AWI-20030300. The seaward boundaries of the COT, that is, the COBs, on profiles AWI-20030400 and AWI-20030500 (Voss & Jokat 2007) can be dated to 51.5 ± 0.2 and 50.1 ± 0.3 Ma, respectively (Fig. 9).

5 OFFSHORE CRUSTAL ARCHITECTURE OF THE EAST GREENLAND MARGIN

In this section, we summarize offshore crustal models derived from seismic refraction modelling, which extend over the southeast and northeast Greenland margins. MCS data were not included, since we focus on velocity models from basement to the depth to the Moho. Therefore, the resolution of the maps is simply based on the resolution of the *P*-wave velocity models. Two major uncertainties might thus affect the reliability of the maps. Navigation data were not available for some seismic lines, for which the locations of the transects were instead digitized from publications. Where endpoints were available, an equidistant interpolation linked the navigation and the model layers along the profiles. This may result in a modest offset of less than 5 km. Uncertainties also result from digitizing crustal models and identifications of layer boundaries, that is, crystalline basement, Moho and high velocity lower crust (HVLC). Here, we assume maximum errors of less than 500 m for layer depths identifications and, therefore, an error of less than 1 km for layer thicknesses. Note, that we performed no crossover corrections for the variations in thicknesses and layer depths observed at profile crossing points, which result from different shot directions and modelling constraints. The gridding algorithm (adjustable tension continuous curvature surface gridding; Smith & Wessel 1990) smoothed these areas of large gradients of layer depths and thicknesses, resulting in deviations between the maps and source model profiles.

Table 4. Wide-angle seismic line numbers of the corresponding *P*-wave velocity models used for this compilation.

Profile ID	Geographic location	Line colour	Reference	Basement (km)	Moho (km)
	Northeast Greenland				
20030200	south GFZ–COT	red	this paper	120–330	170–330
94300	Bredefjord	Green	2	0–210	50–180
20030300	Ardencaple Fjord–COT	Red	This paper	0–365	20–355
20030400	Godthåb Gulf–COT	Red	3	0–313	20–300
94320	Keiser Franz Joseph Fjord	Green	4	0–375	75–250*
20030500	Keiser Franz Joseph Fjord–COT	Red	3	0–465	50–450
94340	Kong Oscar Fjord	Green	4	0–350	87–300
94360	Dickson Fjord	Green	4	0–230	40–200
	Central East Greenland				
94410	Nordvest Fjord–Hall Bredning	Dark blue	5	0–270	50–255
90320	Føn Fjord–Hall Bredning	Dark blue	5	0–210	40–195
94400	Gåse Fjord–Hall Bredning	Dark blue	4,5	0–270	70–250
90537	N–S Hall Bredning	Pink	6	0–116	0–116
90538	W–E Hall Bredning (south)	Pink	6	0–36	0–36
90539	N–S Hall Bredning (southern)	Pink	6	0–85	0–85
90540	N–S Hall Bredning (northern)	Pink	6	0–34	0–34
90549	W–E Hall Bredning (north)	Pink	6	0–42	0–42
90554	W–E Hall Bredning (central)	Pink	6	0–36	0–36
88300	W–E Scoresby Sund–Kolbeinsey Ridge	Orange	7	155–417	155–417
88400	N–S Scoresby Sund (C5)	Orange	7	0–165	0–165
88500	N–S Scoresby Sund (C6?)	Orange	7	0–120	0–120
88600	NE Jameson Land	Orange	7	0–164	0–164
	Kolbeinsey Ridge–Jan Mayen Basin				
L1	N–S eastern flank of Kolbeinsey Ridge	Light blue	8	0–98	0–98
L2	N–S 12 km east of Kolbeinsey Ridge	Light blue	8	0–99	0–99
L3	W–E Kolbeinsey Ridge–Jan Mayen Basin	Light blue	8,9,10	0–284	0–284
L5	eastern Jan Mayen Basin	Light blue	9	0–125	0–125
L6	western Jan Mayen Basin	Light blue	9	0–125	0–125
	Southeast Greenland				
SIGMA I	Greenland–Iceland Ridge	Brown	12	0–500	0–500
SIGMA II	SE Greenland–ocean basin	Brown	11,12	0–350	0–350
SIGMA III	SE Greenland–ocean basin	Brown	12,13	0–391	0–391
SIGMA IV	Southern tip of Greenland	Brown	12	0–348	0–348

Notes: Geographic locations and line colours correspond to lines in Fig. 1. The resolution of the basement and Moho is given in km along the profiles. See references for details of the profiles: (1) Fechner & Jokat (1996); (2) Holbrook *et al.* (2001); (3) Hopper *et al.* (2003); (4) Kodaira *et al.* (1997); (5) Kodaira *et al.* (1998a); (6) Kodaira *et al.* (1998b); (7) Korenaga *et al.* (2000); (8) Schlindwein (1998); (9) Schlindwein & Jokat (1999); (10) Schmidt-Aursch & Jokat (2005a); (11) Voss & Jokat (2007); (12) Weigel *et al.* (1995). Abbreviations of locations are C5,C6? magnetic chrons off Scoresby Sund; COT, continent ocean transition zone; GFZ, Greenland Fracture Zone; N–S, north to south; W–E, west to east; NE, northeast; SE, southeast.

5.1 Seismic profiles

The entire length of the East Greenland margin (∼3000 km) is covered with ∼50 wide-angle seismic profiles, which constrain the crustal structure from the top sedimentary cover to the Moho (Fig. 1). We used a set of crustal models based on 30 wide-angle seismic lines (Table 4). Four lines, SIGMA I–IV (Holbrook *et al.* 2001; Hopper *et al.* 2003; Korenaga *et al.* 2000), cover the area between the Greenland-Iceland Ridge (SIGMA I) and the southern tip of Greenland (SIGMA IV). For these, in situ sample control from ODP drillholes exists (Larsen *et al.* 1994). The quality of the *P*-wave velocity models of SIGMA II–IV is excellent. SIGMA II is based on seismic tomography (Korenaga *et al.* 2000) and layer boundaries were derived from velocity contour lines. Constraints from SIGMA I (Holbrook *et al.* 2001) might contain larger uncertainties due to the moderate quality of the published model.

Between the Greenland–Iceland Ridge (GIR) and Scoresby Sund, that is, offshore the Geikie Plateau (Fig. 1), wide angle seismic data are insufficient for this region to be included in the presented maps.

The region of Hall Bredning and Scoresby Sund is constrained on profiles by several authors (Fechner & Jokat 1996; Mandler & Jokat 1998; Schmidt-Aursch & Jokat 2005a). A selection of six north–south and east–west trending lines (90537-90540, 90548 and 90554) along and across Hall Bredning are included after Fechner & Jokat (1996). These provide a good approximation to the crustal structure in this region. Using the complete set of lines would not change the overview of the East Greenland margin. Velocity models from profiles 94410 (Nordvestfjord), 90320 (Fønfjord) and 94400 (Gåsefjord) were used in this compilation from Schmidt-Aursch & Jokat (2005a), who remodelled previous transects (Mandler & Jokat 1998) with additional recording units.

Weigel *et al.* (1995) present crustal structure models off Scoresby Sund and south of Kong Oscar Fjord. The offshore network of lines 88300–88600 provide good to moderate constraints on the younger oceanic crust from the west flank of the Kolbeinsey Ridge. Moho depths are occasionally weakly resolved. Therefore, a simplified model structure is used for mapping. From the eastern flank of the younger ridge system to the Jan Mayen basin, the crustal structure is imaged by a network of wide-angle lines L1, L2, L3, L5 and L6 from Kodaira *et al.* (1997, 1998a, 1998b).

The crustal structure and the continental sedimentary basins of the Fjord region north of the Jan Mayen Fracture Zone are

resolved by profiles in the Dickson Fjord (94360), Kong Oscar Fjord (94340), Kejser Franz Joseph Fjord (94320) and Brede Fjord (94300) (Schlindwein 1998; Schlindwein & Jokat 1999, 2000; Schmidt-Aursch & Jokat 2005a). Line 94320 is extended in the prolongation of the Keiser Franz Joseph Fjord with profile AWI-20030500. The COT and onset of oceanic crust are imaged by this transect, together with lines AWI-20030400 and AWI-20030300. Profile AWI-20030200 marks the northernmost limit of the East Greenland mapping region. Crustal models of CDP profiles 41, 46 and 61 are excluded (Hinz *et al.* 1987; Mutter & Zehnder 1988) due to their proximity to the higher-resolution profiles AWI-20030200-500.

5.2 Depth to crystalline basement

The top of crystalline basement in the offshore continental parts of the margin is defined at the 6.0 km s^{-1} velocity contour, which is consistent with global studies (Christensen & Mooney 1995). Basaltic layers within the sedimentary units of the COT are not considered as basement units. This yields a maximum discrepancy of 1.2 km between the depth of the 6.0 km s^{-1} contour line and the interpreted basement within the COT on profiles AWI-20030400 and AWI-20030500. In order to be consistent in this compilation, the 6.0 km s^{-1} isopach is used for both the continental and COT domains.

Within the oceanic crust, the top of oceanic layer 2A (White *et al.* 1992) is chosen as the top basement layer. Within the oceanic part of profile SIGMA II, a 4.0 km s^{-1} isopach approximates the top of oceanic basement reasonably well, and is consistent with our seismic profiles of northeast Greenland.

The depth to the basement is mapped over the full extent of the profiles (Table 4), which sum up to almost 6648 km. Fig. 11 illustrates the results. The largest deviations, of up to 6.4 km, occur between the grid and line data near the Shannon High (AWI-20030300). Here, the steep gradient on the eastern margin of the high is smoothed out in the mapped representation of basement depth.

The map clearly shows the relatively uniform and shallow depth to basement in the south compared to the variations in depth of the central to northeast Greenland margin. The deep sedimentary basins observed in Scoresby Sund (Weigel *et al.* 1995) and on Jameson Land (Fechner & Jokat 1996; Schlindwein & Jokat 1999; Schmidt-Aursch & Jokat 2005a) (Figs 1 and 11) die out towards the Jan Mayen Fracture Zone. The central- and northeastern offshore sedimentary basins, which are deeper than 3 km, correlate well with previous publications (e.g. Larsen 1990; Henriksen *et al.* 2000). Voss & Jokat (2007) suggested that the basin north of the Jan Mayen Fracture Zone consists of 4 km of syn-rift sediments mixed with basalts, overlain by post-break-up sediments forming the present day shelf region. Additional constraints on the extent of the >8 km deep sedimentary basins off Shannon Island and further north, outline a change in rifting style between lines AWI-20030400 and AWI-20030300.

5.3 Depth to Moho

The Moho is not resolved at the beginning and end of several seismic lines, due to the lack of ray coverage. In order to minimize extrapolation of unresolved regions, we trimmed the lines to the resolved Moho (Table 4). In all, 5973 km of Moho depth values were used for mapping (Fig. 12). The largest averaging effect occurs at the end of line 94360, at its intersection with profile AWI-20030500. Here, the Moho decreases by ∼3.6 km, which matches reasonably well with the better-constrained Moho of profile AWI-20030500. A slight step in the Moho at kilometres 170–200 of profile 94410 (Schmidt-Aursch and Jokat, 2005a) is smoothed and raised by up to 3.6 km in the grid. A shallower Moho depth of up to 5 km compared to a 3-D gravity model (Schmidt-Aursch & Jokat 2005b) is based mainly on the additional contribution of seismic lines in the Jan Mayen basin after Kodaira *et al.* (1998a) and the new constraints of the COT and oceanic crust from the profiles AWI-20030200–500.

5.4 Crustal thickness

Crustal thicknesses are derived from the line data before interpolation, that is, the difference between the top crystalline basement and the depth to the Moho. Syn- and postrift sediments and basalts are not included and the thickness of the crust was only calculated where Moho depths could be picked. The largest deviations occur as a result of smoothing the basement near the Shannon High of profile AWI-20030300. Moderate variations occur on several other line intersections in the central-east Greenland region most likely due to the different resolutions and interpretations of the profiles and/or steep gradients in the derived thicknesses.

The major differences in the oceanic crustal thickness of the northeastern and southeastern margin are obvious (Fig. 13). Between the Jan Mayen and Greenland fracture zones, oceanic crustal thickness decreases rapidly from 10 to 13 km just east of the COB to normal and even thinner values (7–5 km). Along all profiles of the northeast Greenland margin, a rapid decrease to thinner than normal oceanic crust occurs prior to C21. Igneous crust decreases from 18 to 30 km to ∼8 km thickness along the southern profiles SIGMA-II, -III and IV. C24–C21 aged oceanic crust south of the Greenland-Iceland Ridge (GIR) is up to 5 km thicker than that north of the Jan Mayen Fracture Zone. The extreme crustal thickness of 25–35 km, derived from line SIGMA-I, is clearly associated with the GIR (Holbrook *et al.* 2001), and contrasts with the younger and thinner crust (∼5–10 km) off Scoresby Sund.

5.5 Thickness of high velocity lower crust

Several seismic models in this compilation show a high velocity lower crust (HVLC; velocities exceeding 7.0 km s^{-1}) each of which is associated with increased magmatism during break-up by the corresponding authors. The thickness of the HVLC along the East Greenland margin is illustrated in Fig. 14, ignoring the varying interpretations of it as representing subcontinental pure magmatic underplating (Schlindwein & Jokat 1999; Voss & Jokat 2007), igneous transitional crust and/or thickened oceanic crust (Weigel *et al.* 1995; Kodaira *et al.* 1997; Kodaira *et al.* 1998a; Kodaira *et al.* 1998b; Korenaga *et al.* 2000; Holbrook *et al.* 2001; Hopper *et al.* 2003). None of these authors suggested the possibility of serpentinized mantle or eclogitic material, which display similar high seismic velocities and density anomalies and have been considered as alternatives to magmatic layers beneath the Norwegian margin (Mjelde *et al.* 2002; Gernigon *et al.* 2003; Ebbing *et al.* 2006; Gernigon *et al.* 2004). Major misfits and averaging occurred at the Keiser Franz Joseph Fjord between lines 94320, 94360 and AWI-20030500 at the landward end of the HVLC. Schlindwein & Jokat (1999) resolved high velocities only at the end of the lines while Voss & Jokat (2007) imaged the full extent of this body. However, gridding causes a reduction of the thickness by 3.1–6.4 km between km 60

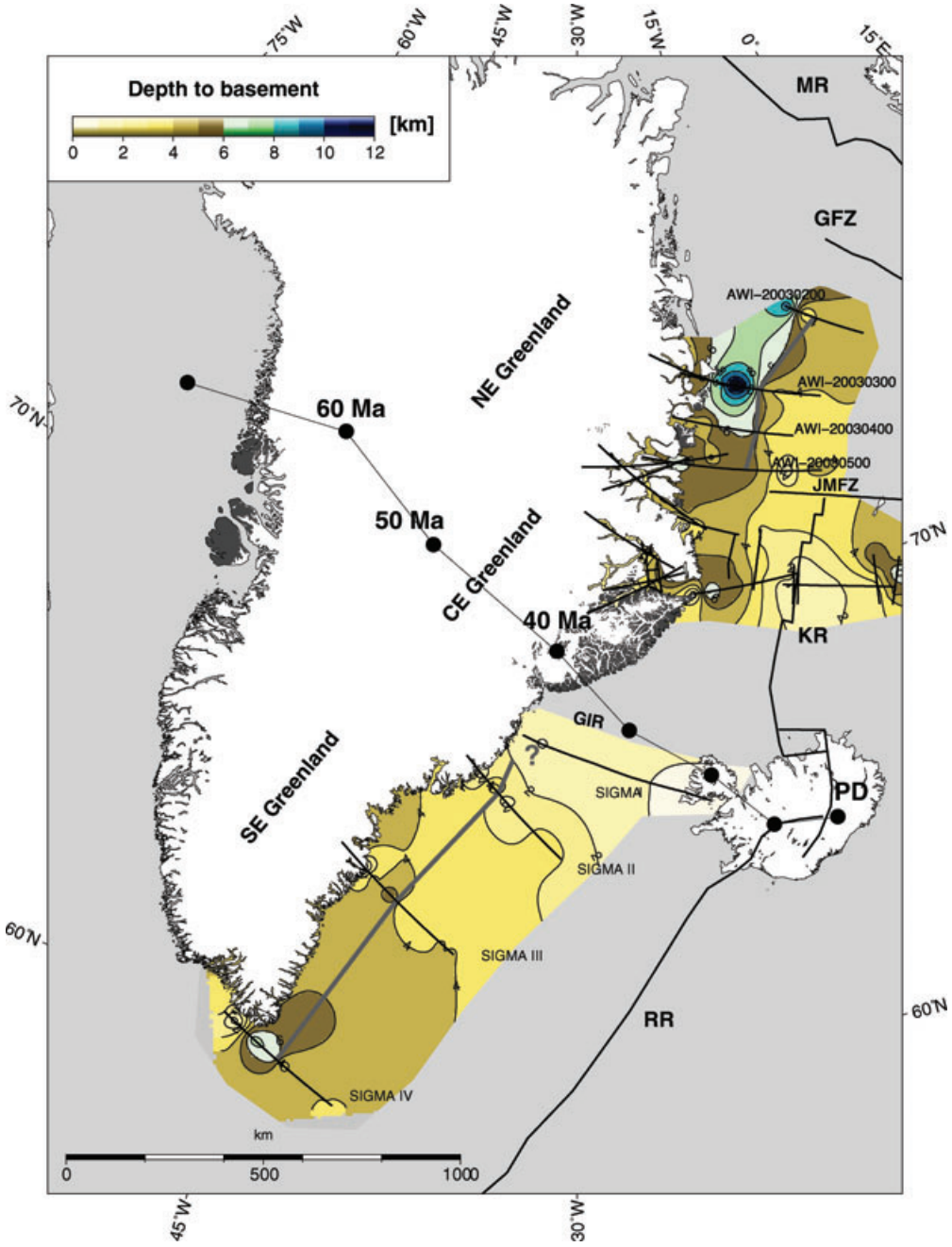

Figure 11. Map of generalized depth to crystalline basement based on published seismic lines shown in Fig. 1 and listed in Table 4. Basement is defined at the 6.0 km s^{-1} contour line in the continental domain, and at the top of oceanic layer 2A in the oceanic domain. Onshore dark grey regions mark flood basalts. Outline of mapped region excludes large scale extrapolations. Contours every 1 km are included as reference. Thick grey line marks the break-up location along the SIGMA profiles in Southeast Greenland after Holbrook *et al.* (2001). Question mark denotes unknown location of the line of break-up. The same line marks the seaward COB of the transition zones as in Fig. 8 along profiles AWI-2003200–500 in northeast Greenland. Black lines mark profile locations. Abbreviations are as in Fig. 1. Scale is valid for 70° N.

and 75 on profile AWI-20030500 (Fig. 9). Misfits of less than 3.5 km occur locally near the Kolbeinsey Ridge (88300 and L1), the extension of the Kong Oscar Fjord (94360 and 88600) and on lines SIGMA-I, -III and -IV (Fig. 1).

The map shows strong variations in the dimensions of the HVLC, with two different styles. The southern margin shows a widespread high velocity lower crust. The moderate to great thicknesses of 5–10 km (SIGMA II–IV) underlie the oceanic crust as well as landward of the COB. A maximum thickness of 15 km is reached along the GIR (SIGMA-I). No HVLC was identified within the continental crust of Hall Bredning and Scoresby Sund (Fechner 1994; Schlindwein & Jokat 1999; Schmidt-Aursch & Jokat 2005a) (Fig. 1), and there is insufficient seismic coverage to image the lower crust beneath the basalt-covered Geikie Plateau. The young oceanic crust west of the Kolbeinsey Ridge, however, contains a 5–10 km thick HVLC (Weigel *et al.* 1995), greater than on the eastern side of the ridge, where it decreases to less than 5 km (L1–L6) (Kodaira *et al.* 1998a; Kodaira *et al.* 1997; Kodaira *et al.* 1998b).

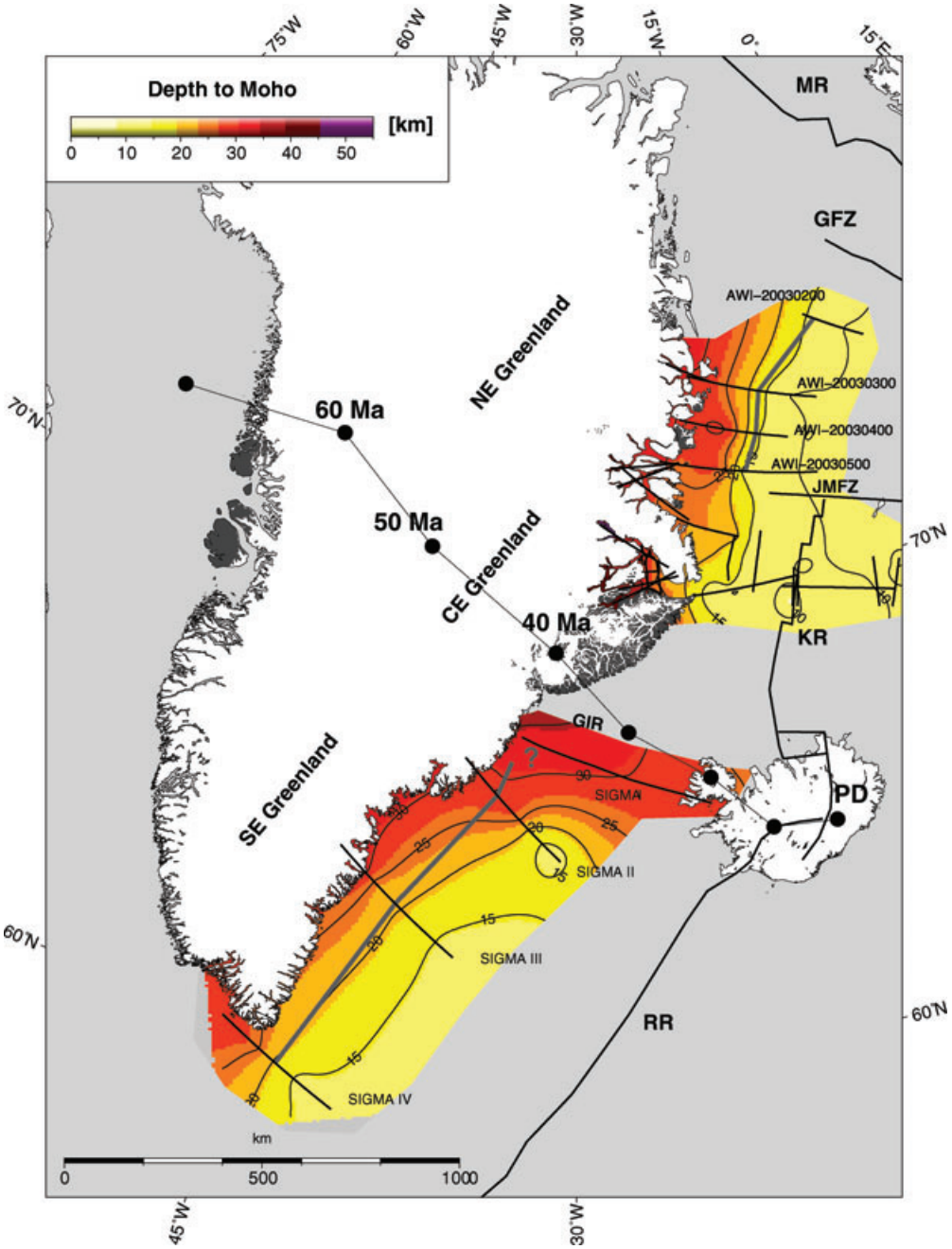

Figure 12. Map of depth to Moho. Moho depths are only used where constrained by ray coverage or outlined in other published models. In general it coincides with the 8.0 km s^{-1} velocity contour line. Depth contours are outlined every 5 km. Format of map is equivalent to Fig. 11.

Near the Jan Mayen Fracture Zone, and further north, the pattern of the high velocity lower crustal thickness shows more variations with great local maxima which probably is due to the more closely spaced data. The HVLC identified on the Kong Oscar Fjord profile 94360 (Schlindwein & Jokat 1999) (Fig. 1) increases from 5 km thickness to a maximum of 15 km on the nearby profile 88600 (Weigel *et al.* 1995), where almost the entire oceanic crust contains velocities of greater than 7.0 km s^{-1}. North of the fracture zone, the maximum thickness of the HVLC exceeds 10–15 km (AWI-20030400 and AWI-20030500) (Voss & Jokat 2007), and is found landward of and along the COT, with a strong decrease in thickness towards the onset of oceanic crust and towards the north. From C23 and C22 eastwards, no high velocity oceanic layer (>7.0 km s^{-1}) appears in the seismic models. This is in strong contrast to the southern margin, where the oceanic crust apparently has a high velocity lower layer of more than 5 km thickness at similar crustal ages.

6 DISCUSSION

The heterogeneous style of the northeast Greenland margin domain differs significantly from the more regular style in the southeastern domain in almost all maps. This might be influenced by the much smaller distance between northern seismic lines and the spatial extent of about 800 km from the Scoresby Sund to the northern end compared to almost 1200 km along the southeastern margin. The

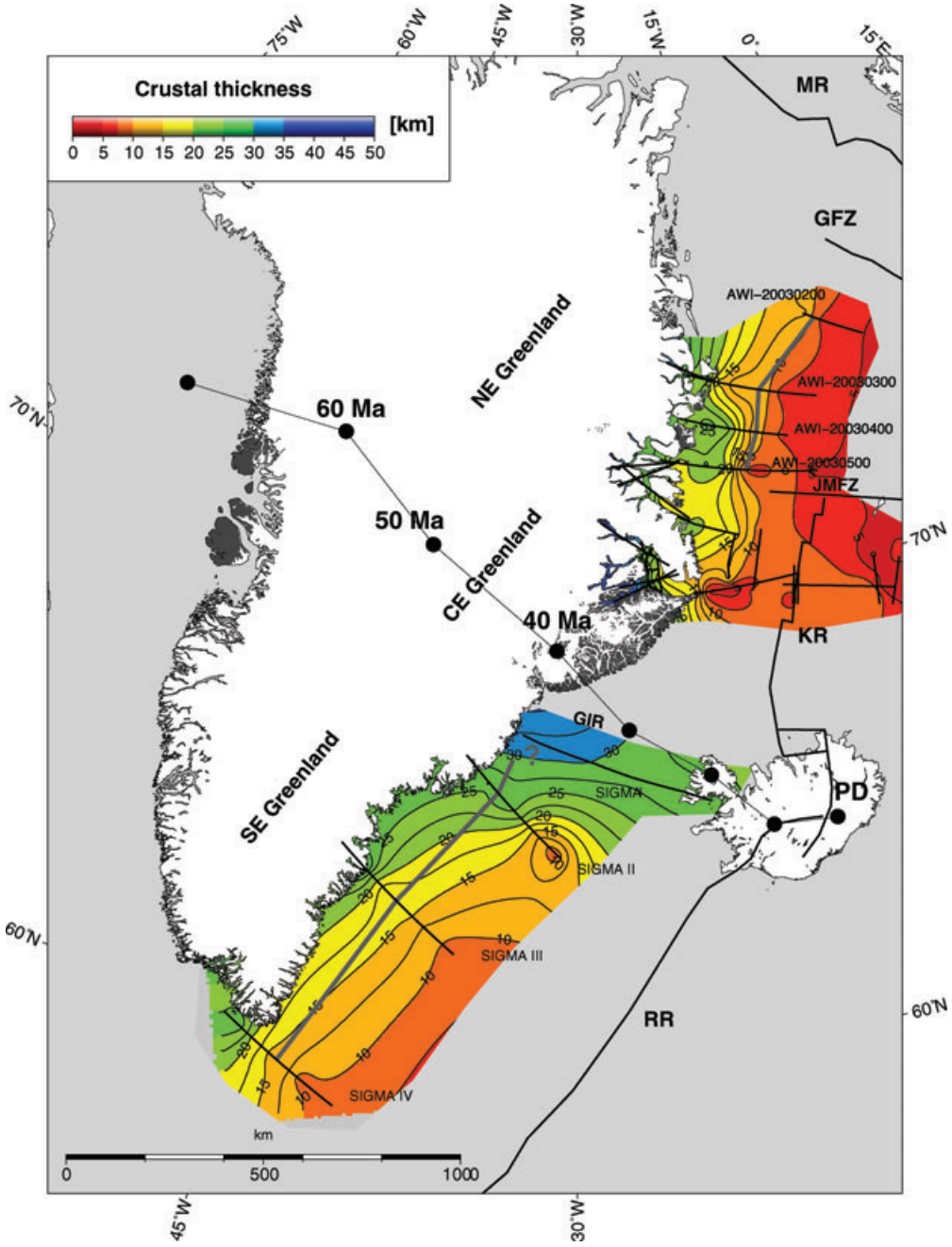

Figure 13. Crustal thickness map, with thicknesses calculated from line data (Moho–basement) prior to mapping. Contour lines every 2.5 km. Note the different thicknesses seaward of the grey line in the northeast and southeast Greenland margins. Format of map is equivalent to Fig. 11.

maps emphasize, however, the strong variations of the northern and southern regions in terms of the dimension, distribution and extent of the HVLC, and the thickness of the oceanic crust.

The presented profiles are all located within a radius of ∼1300 km from the proposed location of the Iceland plume track (Lawver & Müller 1994). Despite the similar distances of the seismic lines AWI-20030200-500 and SIGMA I–IV to the Icelandic thermal anomaly, the heterogeneous distribution of the HVLC along the Greenland margins suggests strong variations in margin formation processes. The first major difference is that the majority and maxima of the HVLC are interpreted as pure magmatic underplating beneath extended continental crust (Voss & Jokat 2007) near the Jan Mayen Fracture Zone, but HVLC is absent only 100 km further to the north, where only minor intrusions appear near the COB. Emplacement of high velocity igneous crust landward of the COB is less for the southern Greenland region, but continues much further out into the transitional and oceanic domains.

The second difference is in the maximum thickness of the HVLC. SIGMA II–IV lines show an almost continuous distribution of the HVLC and its thickness while in the north it appears more concentrated on the vicinity of the Jan Mayen Fracture Zone (Fig. 14), where it is less widespread but almost twice as thick as off southeast Greenland.

The third major difference is the thickness age and content of the oceanic HVLC. Between break-up and C21 (47.1 Ma) (C21 marked in Fig. 14), the oceanic crust in the northern region loses

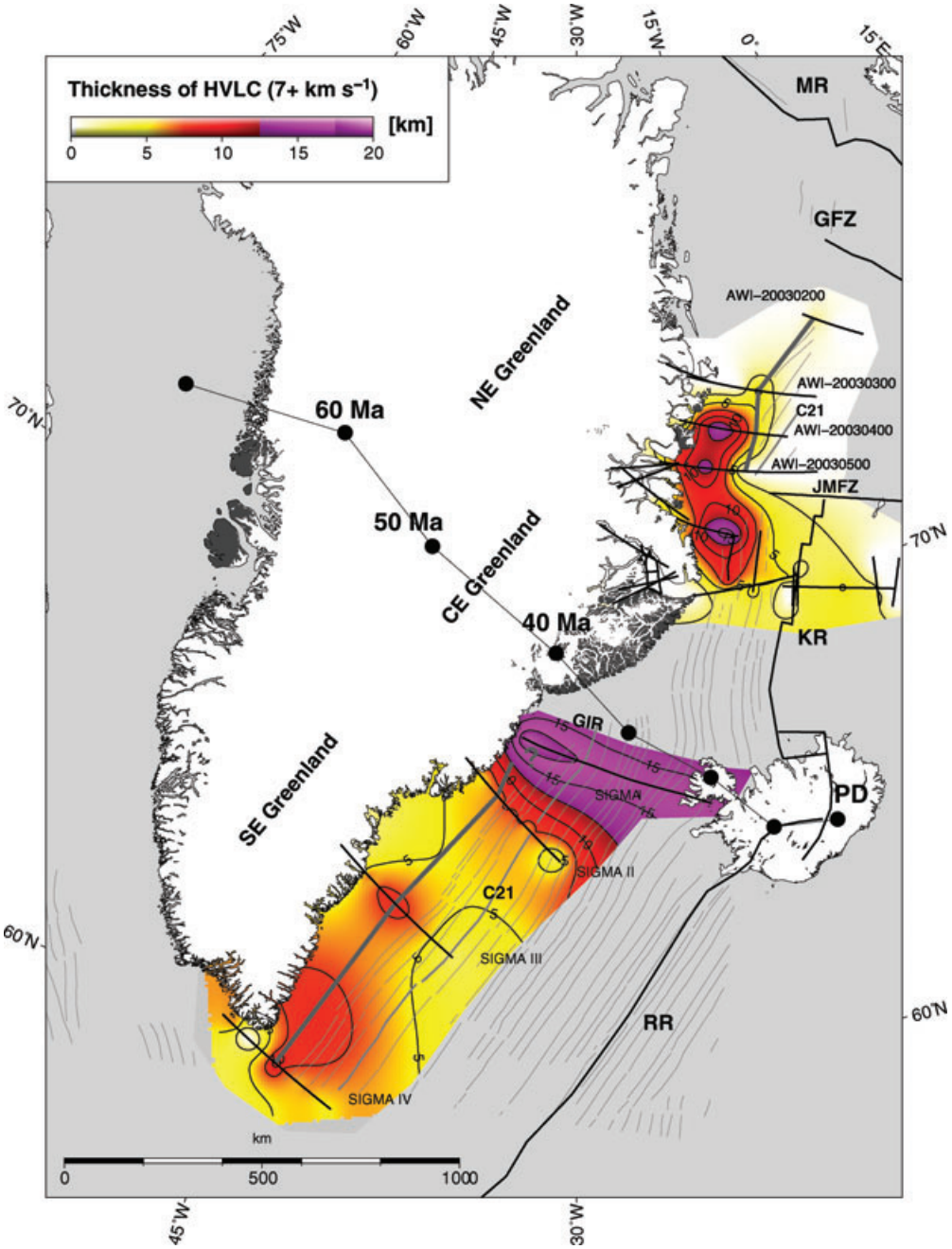

Figure 14. Thickness map of high velocity lower crust (HVLC), including seismic velocities of >7.0 km s^{-1} along the East Greenland margin. It includes igneous crust and subcontinental magmatic underplating. Contour interval 2.5 km. Magnetic spreading anomalies are included and C21 is highlighted for reference. Note the different distributions of the thicknesses between southeast and northeast Greenland. Format of map is equivalent to Fig. 11.

its HVLC and thins rapidly to about 5 km. Off southeast Greenland, the oceanic crust near C21 still has a HVLC and its thickness is in the range 8–10 km.

6.1 HVLC distribution at North Atlantic conjugate margins

Regional melt distribution prior to and shortly after break-up along the East Greenland and conjugate margins can be estimated from HVLC thicknesses. Average thicknesses are estimated for the East Greenland margin landward of the line of break-up (Holbrook *et al.* 2001), and the proposed northeastern COB (Figs 9 and 14), and out to magnetic chron C21 for the oceanic domain. The distances of the East Greenland margin profiles from the plume head are related to SIGMA I (Fig. 14) which is located along the Greenland–Iceland Ridge (GIR). The contributions of profiles 94340 and 88600 (Weigel *et al.* 1995; Schlindwein & Jokat 1999) are included, even if this region is influenced by Late Oligocene to Miocene rifting. Profile Cam77 (Barton & White 1995) of the Edoras Bank margin (EB) and line NI8 from Hatton Bank (HB) (Fowler *et al.* 1989; Morgan *et al.* 1989) are appropriate conjugate transects for the southeast Greenland margin (Holbrook *et al.* 2001; Hopper *et al.* 2003). Profiles OBS-99 from the Vøring margin (Mjelde *et al.* 2005) and T1 from the Lofoten margin (Tsikalas *et al.* 2005), as previously

shown (Voss & Jokat 2007; this paper), are conjugate to the northeast Greenland lines (Fig. 8). Spatial distances on the conjugate margin are related to the Faeroe-Iceland Ridge (FIR) (Bott & Gunnarson 1980), the eastward prolongation of the GIR according to Barton & White (1995). These authors suggest a symmetric distribution of excess melt thickness north and south of the FIR. The decreased melt thicknesses at the peripheries of the region indicate decreased asthenospheric temperatures with increasing distance to the plume location. An increased temperature of approximately 100 °C associated with the Iceland plume is assumed to result in passive upwelling and the emplacement of large amounts of melt compared to the succeeding oceanic crust. Considering subcontinental and oceanic HVLC thicknesses separately, a surprising inversion of the melt distribution appears (Fig. 15). The general trend of decreasing melt volume away from the plume (GIR and FIR) is marked by asymmetry. Thicker HVLC landward of the COBs opposes thinner oceanic HVLC increasingly to the north. The strong northward decrease is displayed on both margins, as previously commented.

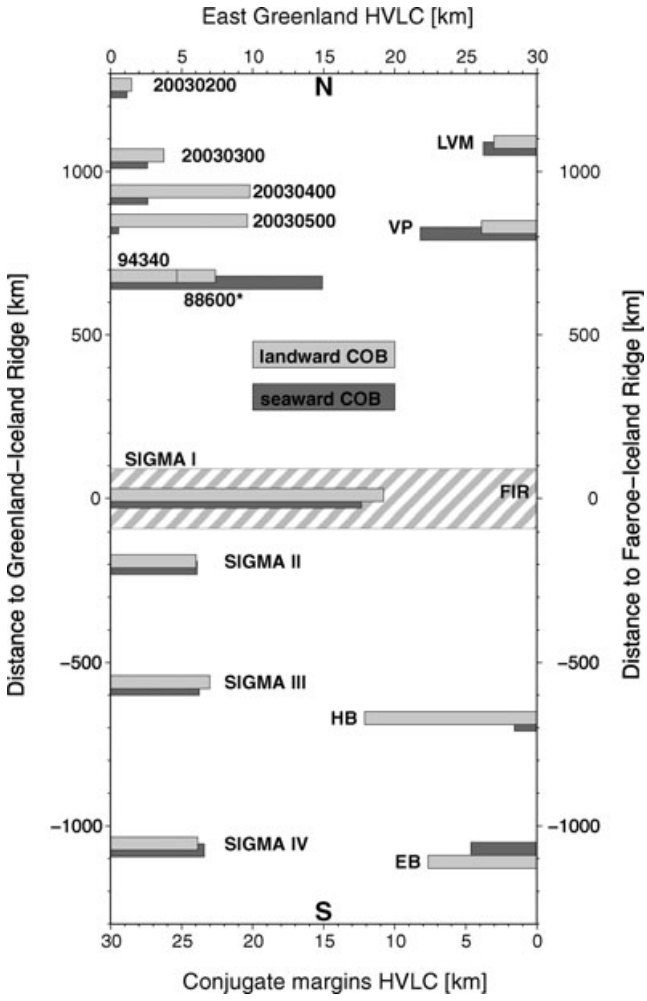

Figure 15. N–S distribution of HVLC thicknesses of East Greenland and conjugate margin transects. Separation of landward and seaward portions according to associated COBs. Distances are related to SIGMA I location near the Greenland Iceland Ridge for the East Greenland side and to the Faeroe-Iceland Ridge for conjugate profiles. Abbreviations are COB: Continent–ocean boundary, EB: Edoras Bank, FIR: Faeroe-Iceland Ridge, HB: Hatton Bank, LVM: Lofoten-Vesterålen Margin, VP: Vøring Plateau. Asterisk mark profile across oceanic crust of different age than others. See text for details.

The southern regions reveal, even for the distal regions, moderate average thicknesses landwards of the COBs. However, peak values of subcontinental HVLC content appear only locally distributed and seems to have a much smaller spatial extent north of the Jan Mayen Fracture Zone (Figs 14 and 15). The outstanding HVLC thickness in the oceanic domain at 670 km (profile 88600) (Figs 14 and 15) correlates with the margin segment that was involved in the separation of the Jan Mayen microcontinent and the early spreading of the Kolbeinsey Ridge (Weigel *et al.* 1995). The heterogeneous distribution of the HVLC suggests, however, different sources of melt generation and emplacement. The width of transition zones and the spatial extent of decreasing thickness of the HVLC has also been shown as strongly asymmetric off conjugate margins (e.g. Hopper *et al.* 2003; Voss & Jokat 2007), which has important implications for volumetric magma quantifications associated with the opening of the North Atlantic (Eldholm & Grue 1994).

6.2 Northeast Greenland melt distribution and margin formation models

In general, the observed structural styles of the North Atlantic volcanic margins are associated with the influence of a mantle plume and two end-member melt generation models exist (e.g. White & McKenzie 1989; Kelemen & Holbrook 1995; Holbrook *et al.* 2001; Korenaga *et al.* 2002). Passive upwelling is understood to produce thicker high velocity crust at higher temperatures from deep-seated melt generation in the mantle that results in enriched MgO content. Melt generation from shallower mantle regions and a moderate thermal anomaly in response to active upwelling produce no substantial crustal velocity variations. The development of the southeast Greenland margin was proposed to be influenced by a hotspot (Holbrook *et al.* 2001) or thin spot (Hopper *et al.* 2003) with proximal active upwelling (SIGMA I and II). Passive upwelling and a decrease of the thermal anomaly from break-up to C21/C20 is inferred for the regions of SIGMA III and IV from the crustal thicknesses and bulk velocities. Lateral flow of warm material to distal areas (Sleep 1996) was supposed to reach the southern tip of Greenland (Holbrook *et al.* 2001), a distance of ∼1200 km, and to be responsible for the thick oceanic crust there. Exhaustion of the thermal anomaly at 45 Ma and the reduction of the plume head radius from ∼300 km to less than 200 km reduced the production of high velocity lower oceanic crust and igneous crustal thickness (Holbrook *et al.* 2001; Hopper *et al.* 2003). To the north, similar distances from the possible plume location at 56 Ma, or indeed from the present-day Iceland thermal anomaly, would extend beyond profile AWI-20030200. But, it has been shown that the HVLC distribution differs substantially in such a way that large scale magmatism is almost absent at the northern periphery. Mjelde *et al.* (2003) postulated intervening active and passive rifting components from the regional structural styles of the Vøring margin. The decrease of magmatism with increasing plume distance is consistent with an active portion. The proposal that crustal lineaments acted as barriers to melt emplacement, documents the passive component. Local indications of HVLC thickness and velocity variations have also been related to a heterogeneous asthenospheric source. Three hypothetical models are considered to explain our observations from the northeast Greenland margin.

Model 1–Pre-Palaeogene long-term rifting and melt accumulation from one major feeder dyke

The northeast Greenland margin includes highly extended continental crust together, locally, with large scale magmatism. Similar highly extended continental crust exists for about 100 km further

north. Excess magmatism seems there, however, restricted to the point of break-up and is almost absent near the Greenland Fracture Zone. Slow rifting is generally associated with minor melt production due to conductive cooling during rifting (Bown & White 1995), consistent with the observations off Shannon Island (AWI-20030300). Thus, slowly rifting and crustal thinning is assumed to have started long before the Tertiary magmatic event. We deduce from the above analysis that the direct influence of a mantle plume head, active upwelling, wide spread lower crustal magma flows, and/or other proposed models seem plausible explanations for the southern region of the East Greenland margin. We therefore, assume for this model that a feeder dyke, originating from the distal plume head, sufficiently supported magmatism into the region of the increased HVLC north of the Jan Mayen Fracture Zone (AWI-20030400/500). The decrease in magmatism and variations in the HVLC along the northeast Greenland margin suggest, in this case, the existence of a lithospheric- scale melt barrier. The different structural styles between the margins covered by AWI-200400/500 and AWI-20030300 let assume the existence of a transfer zone or a lithospheric detachment that might acted as a barrier to the Tertiary magmatism. This region marks a transition from the highly volcanic margin in the south (AWI-20030400/500) to magma-poor rifting and break-up further north. Assuming the HVLC of the two southern profiles is the result of pure magmatic underplating, that is, subtracting it from the total crustal thickness, a pre-magmatic Moho is much shallower than on the northern profile (Fig. 9). By contrast, a greater basin depth appears in the north lying along the prolongation of major Caledonian extensional detachments known from onshore observations (Hartz *et al.* 2002). The thick portion of magmatic underplating can then be interpreted as an accumulation-point of Tertiary magmatism, where Moho depths were lowest. Melt migration or lower crustal flow, as proposed for southeast Greenland, might probably have been channelled away from the thick continental crust and the Caledonian root structure to the west (Schmidt-Aursch & Jokat 2005b) and the transfer zone/detachment to the north. Conductive cooling decreased upper mantle temperatures and the amount of igneous crustal accretion following the initiation of seafloor spreading, which explains the rapid decrease in oceanic crustal thickness. Such a model has some similarities with the edge driven small scale convection model of King & Anderson (1995, 1998) or the soft spot model of Callot *et al.* (2002); Tsikalas *et al.* (2002) proposed a conjugate transfer zone system along the East Greenland margin, based on regional magnetic data and the projections of major structures on the Norwegian margin. The extents of profiles AWI-20030200-400 should cross these proposed features but no evidence for them is found on the seismic lines. Recent publications of potential field data from the Norwegian-Greenland Sea also show little evidence for the previously proposed lineaments and fracture zones on both sides of the North Atlantic (Ebbing *et al.* 2006; Olesen *et al.* 2007). However, a major detachment fault between Godthåb Gulf and Ardencaple Fjord (Shannon Island) could explain the sudden decrease of magmatic underplating to the north and find support from the presented different structural styles.

Model 2–Highly intruded thick continental crust and several small feeder dykes

Magmatic production from several small scale local volcanic feeders at the northeast Greenland margin might explain the larger thickness but smaller spatial extent of the HVLC, compared to the southeast Greenland margin. The thickness of the HVLC shows large gradients in all directions, while along the southeast Greenland margin it is distributed more homogeneously (except for the increase towards the Greenland Iceland Ridge). Voss & Jokat (2007) classified the HVLC as Tertiary magmatic underplating, which is a reasonable explanation according to previous interpretations of the region and the conjugate margin (Mjelde *et al.* 2002; Mjelde *et al.* 2005; Schlindwein & Jokat 1999). Supporting arguments come from the increased velocities and densities, the distinct top reflector and Moho reflections, the shallower basin depth compared to the adjacent margin segments and the complex magnetic anomaly pattern offshore and prior to the ocean spreading anomalies. Interpreting the HVLC instead as highly intruded lower crust including components of continental crust, addresses the same arguments but qualifies the delay between magmatism and break-up. The difference here is that the HVLC is not attributed to a pure magmatic body ponded beneath highly thinned continental crust. Instead, several small scale feeder dykes penetrate the rifted continental crust, and the top lower-crustal reflections are related to major sills. Small volcano-like features occur at km 220 and 190 on profiles AWI-20030400 and AWI-20030500 respectively (Fig. 9) (Voss & Jokat 2007). The magnetic anomaly pattern can be attributed to the magmatic lower crustal intrusions. The increased Cenozoic sediment thicknesses on these profiles are a result of isostatic subsidence due to the weight of the intruded crust compared to AWI-20030300. Minor volcanism occurred further north, at Shannon Island. The strong decrease in oceanic crustal thickness might be seen as a result of decreasing mantle temperature after break-up (Barton & White 1995), but also supports the possibility of more localized volcanism rather than large scale plume-related magma flow. The difference of the HVLC content in the oceanic domain also supports a significantly smaller northern melt generation.

Although this model seems plausible, it has difficulties explaining why the top reflector of the HVLC clearly dips towards the west and whether sills can cause such clear reflections in the lower crust. Additional work like a comprehensive subsidence analysis, which investigates the thermal-tectonic subsidence of the COT, might help to understand whether it subsided due to intrusions or if it was uplifted due to underplating. Evidence of sediment erosion during latest Cretaceous to earliest Palaeocene exhumation has been found in the onshore fjord region (Hartz *et al.* 2002) which would, however, support uplift due to underplating.

Model 3–Secondary magmatic event according to the Jan Mayen separation

Price *et al.* (1997) dated tholeiitic basalts on Traill Ø and related these to the Iceland plume magmatic event (∼54 Ma). A second alkaline magmatic event dated to ∼36 Ma is proposed to have been regionally significant in East Greenland. Slightly younger plateau basalts (∼33 Ma; Upton *et al.* 1995) were found on Hold with Hope. Despite the difference in measurement techniques, it seems obvious that increased magmatism occurred between the onset of spreading along the Kolbeinsey Ridge and the final separation of Jan Mayen (Gudlaugsson *et al.* 1988). This process could explain the localized distribution of the HVLC north and south of the Jan Mayen Fracture Zone, which appears almost symmetrical (Kodaira *et al.* 1997; Kodaira *et al.* 1998a; Voss & Jokat 2007; Weigel *et al.* 1995). This model implies that the initial crustal structural style might have been similar to the model off Shannon Island. The primary magmatic event revealed intrusions during extension and the formation of onshore plateau basalts. Break-up occurred along the northeast Greenland margin between 54 and 50 Ma (Fig. 9), emplacing SDRS (Hinz *et al.* 1987; Mutter & Zehnder 1988). The second event started with initiation of the Kolbeinsey Ridge system and the separation of the Jan Mayen microcontinent (Gudlaugsson *et al.* 1988). Thick

oceanic crust accreted to the central-east Greenland margin south of the Jan Mayen Fracture Zone. Ascending melt ponded beneath the primary sealed and thinned continental crust (COT of AWI-20030400 and 500) and formed the local thick magmatic underplate there. The complex magmatic pattern is therefore attributed to primary intrusions. If the secondary magmatic underplating contributes the magnetic anomalies depends on the depth-level of the Curie temperature. The resulting uplift might have caused erosion of the early basalts on- and offshore, which suggests that the shelf region might have had a widespread cover of flood basalts, similar to the flood basalts exposed on the Geikie Plateau (Fig. 1). According to this model, the observed underplating from Kong Oscar Fjord, Kejser Franz Joseph Fjord and Godthåb Gulf is most likely related to Late Eocene rather than Late Palaeocene/Early Eocene magmatism. The melt production affects margin formation in a small radius of less than 200 km, leaving the region off Shannon Island and south of Scoresby Sund unaffected. A difficulty of this model is the explanation of the thinner oceanic crust off Kejser Franz Joseph Fjord, which is conjugate to the Kolbeinsey Ridge across the Jan Mayen Fracture Zone.

The models presented form three end-members. Some combination of these might best describe the evolution of the northeast Greenland margin. These models contrast with those for the formation of the southeast Greenland margin, emphasizing the strong variations along East Greenland. Plate reconstruction models need to invoke such variations and the asymmetries of conjugate margins, since they have a significant impact in the evaluation of the timing of magmatism, melt quantities, rift durations (e.g. Hopper *et al.* 2003), uplift history (e.g. Clift *et al.* 1995) and the hydrocarbon potential of offshore continental margin basins (Hinz *et al.* 1993). Lithospheric-scale inhomogeneities must be responsible for the heterogeneous melt distribution according to the variations and inversion of the HVLC distribution in continental and oceanic domains, and differences in its velocities (Figs 14 and 15). However, whether or not a mantle plume or other processes are responsible, melt production seems difficult to deduce from geometrical and velocity constraints alone.

7 CONCLUSION

New crustal structure models based on wide-angle seismic data are presented, and 30 seismic models from the southern tip of Greenland to the Greenland Fracture Zone in the north were used to compile maps for regional seismic interfaces within the crust.

Interpretation of *P*-wave velocity models of the profiles AWI-20030200 and AWI-20030300 revealed important constraints on the extent of magmatism along the northeast Greenland margin between the Jan Mayen and Greenland fracture zones. Significant variations were found in the presented models, and the previous published structural models of the two southern profiles AWI-20030400 and AWI-20030500 (Voss & Jokat 2007). The main results are as follows:

1. Between the present-day coastline and shelf edge, there is a significant variation in crustal architecture beneath the basaltic layers that form the volcanic province of the East Greenland margin. A sedimentary basin up to 15 km deep and with a low velocity gradient, and crustal layer with with only higher velocities near the COB define a completely different weak-magmatic evolution of the northeastern margin compared to the highly magmatic evolution of the southern profiles. The continental lithosphere is proposed to have been only sparsely penetrated by melts and not to have been magmatically underplated, whereas excess volcanism further south was voluminous. This difference correlates with the magnetic record along the profiles within these regions. However, Moho depths along the three transects across the northeast margin seem similar, decreasing from 30 km to almost 10 km at the onset of oceanic crust, albeit strongly depending on the width and thickness of the HVLC.

2. The thicknesses of the Cenozoic sediments differ between profiles AWI-20030300, AWI-20030400 and AWI-20030500 across the present day shelf region. Along AWI-20030300 they gradually thicken up to 2.7 km towards the shelf slope, while on the two southern profiles, the sediments have an almost constant thickness of 2.5–3 km. This variation might be linked to variations in subsidence and uplift caused by different magmatic processes, as shown by the observed variability in crustal structure.

3. A significant velocity anomaly is observed underneath the Shannon High, but not on the two southern profiles. The absence of a significant HVLC beneath the Shannon High and the COT, and a positive magnetic anomaly rather than a chaotic magnetic signature as in the south leads us to conclude that the emplacement of plateau basalts on Shannon Island was probably related to a local volcanic event, which was independent from the emplacement of the upper and lower plateau lava sequences on Wollaston Foreland and Hold with Hope (Watt 1994).

4. Oceanic crustal thicknesses in the Greenland Basin decrease slightly towards the north and away from the COB, from approx. 9–13 km at break-up to almost 5 km near chron C21.

5. Half spreading rates were calculated along the four seismic lines between the Greenland and Jan Mayen fracture zones and provide age constraints on the time of break-up. The rates suggest that break-up propagated from north to south in the period from ∼54 to ∼50 Ma, based on identifications of the seaward COBs.

A line-to-line comparison with a crustal transect across the conjugate Lofoten margin reveals surprising similarities in the structural style despite the presence of a unique major tectonic feature, the Lofoten core-complex.

A systematic compilation of 30 crustal models from wide-angle seismic lines along the entire East Greenland margin yields a regional crustal image and its variations. The major differences are the interpretation of the HVLC as pure magmatic underplating and/or accretion seaward of the COB, the distribution of the maximum high velocity lower crust and the thickness of the oceanic crust north and south of Iceland. We demonstrate that the average thicknesses of the HVLC landward and seaward of proposed COBs differs inversely from north to south from the East Greenland margin profiles and their conjugate counterparts when plotted according to their distance from the Greenland-Iceland-Faeroe Ridge.

From this heterogeneous distribution we deduced three possible models for melt generation at the northeast Greenland margin. The first model infers a major feeder dyke linked to the plume head and a transfer zone/detachment between Godthåb Gulf and Shannon Island. A second model suggests thicker continental crust, rather than pure magmatic underplating, and volcanism sourced from several small feeder dykes. The third model involves a second magmatic event which is associated with the separation of the Jan Mayen microcontinent and the formation of the Kolbeinsey Ridge system.

ACKNOWLEDGMENTS

Data acquisition along these profiles was supported by the Deutsche Forschungsgemeinschaft. Funding was provided for data

processing of the wide-angle seismic lines by Statoil and by the European Science Foundation within the EUROMARINS project. We thank John Hopper who provided the digital velocity models of the SIGMA II–IV profiles. The manuscript was improved greatly by comments from Daniela Berger, Erik Lundin, Asbjørn Breivik and Graeme Eagles. We thank Bob Trumbull, Robert White and two anonymous reviewers for their inspiring comments. All figures were created with GMT (Wessel & Smith 1998). Seismic velocity models were created with *RAYINVR* provided by Collin Zelt (Zelt & Smith 1992). 2-D gravity modelling was performed with the commercial software *LCT* provided by *Fugro.*

REFERENCES

Anderson, D.L., 2000. The thermal state of the upper mantle; no role for mantle plumes, *Geophys. Res. Lett.,* **27,** 3623–3626.

Barton, A.J. & White, R.S., 1995. The Edoras Bank continental margin: continental break-up in the presence of a mantle plume, *J. geol. Soc. Lond.,* **152,** 971–974.

Bott, M.H.P. & Gunnarson, K., 1980. Crustal structure of the Iceland-Faeroe Ridge, *J. Geophys.,* **47,** 221–227.

Bown, J.W. & White, R.S., 1995. Effect of finite extension rate on melt generation at rifted continental margins, *J. geophys. Res.,* **100,** 18,011–018,029.

Breivik, A.J., Verhoef, J. & Faleide, J.I., 1999. Effect of thermal contrasts on gravity modeling at passive margins: results from the western Barents Sea, *J. geophys. Res.,* **104,** 15293–15311.

Breivik, A.J., Mjelde, R., Faleide, J.I. & Murai, Y., 2006. Rates of continental breakup magmatism and seafloor spreading in the Norway Basin-Iceland plume interaction, *J. geophys. Res.,* 111.

Callot, J.P., Geoffroy, L. & Brun, J.P., 2002. Development of volcanic passive margins: three-dimensional laboratory models, *Tectonics,* **21,** 1052–1064.

Cande, S.C. & Kent, G.M., 1995. Revised calibration of the geomagnetic polarity timescale for the Late Cretaceous and Cenozoic, *J. geophys. Res.,* **100,** 9761–9788.

Christensen, N.I. & Mooney, W.D., 1995. Seismic velocity structure and composition of the continental crust: a global view, *J. geophys. Res.,* **100,** 9761–9788.

Clift, P.D., Turner, J. & Party, O.D.P.L.S., 1995. Dynamic support by the Iceland plume and vertical tectonics of the northeast Atlantic continental margins, *J. geophys. Res.,* **100,** 24473–24486.

Ebbing, J., Lundin, E., Olesen, O. & Hansen, E.K., 2006. The mid-Norwegian margin: a discussion of crustal lineaments, mafic intrusions, and remnants of the Caledonian root by 3D density modelling and structural interpretation, *J. Geol. Soc., Lond.,* **163,** 47–49.

Eldholm, O. & Grue, K., 1994. North Atlantic volcanic margins: dimensions and production rates, *J. geophys. Res.,* **99,** 2955–2968.

Eldholm, O., Thiede, J. & Taylor, E., 1989. Evolution of the Vøring volcanic margin, *Proc. Ocean Drill. Prog. Sci. Res.,* **104,** 1033–1065.

Escher, J. & Pulvertaft, T., 1995. Geological Map of Greenland, 1:2 500 000, *Geol. Sur. Greenland*.

Fechner, N., 1994. Detailed refraction seismic investigations in the inner Scoresby Sund / East Greenland, in *Reports on Polar and Marine Research,* pp. 1–196, Alfred Wegener Institute of Polar and Marine Research, Bremerhaven.

Fechner, N. & Jokat, W., 1996. Seismic refraction investigations on the crustal structure of the western Jameson Land basin, east Greenland, *J. geophys. Res.,* **101,** 15867–15881.

Foulger, G.R. & Anderson, D.L., 2005. A cool model for the Iceland hotspot, *J. Volcanol. Geother. Res.,* **141,** 1–22.

Fowler, C.M.R., 2005. *The Solid Earth: An Introduction to Global Geophysics,* 2nd ed., Cambridge University Press, Cambridge, UK.

Fowler, S.R., White, R.S., Spence, G.D. & Westbrook, G.K., 1989. The Hatton Bank continental margin—II. Deep strucutre from two-ship expanding spread seismic profiles, *Geophys. J. Int.,* **96,** 295–309.

Funck, T., Hopper, J.R., Larsen, H.C., Louden, K.E., Tucholke, B.E. & Holbrook, W.S., 2003. Crustal structure of the ocean-continent transition at Flemish Cap: seismic refraction results, *J. geophys. Res.,* **108,** 2531–2551.

Funck, T., Jackson, H.R., Louden, K.E., Dehler, S.A. & Wu, Y., 2004. Crustal structure of the northern Nova Scotia rifted continental margin (eastern Canada), *J. geophys. Res.,* **109**.

Gernigon, L., Ringenbach, J.C., Planke, S., Le Gall, B. & Jonquet-Kolstø, H., 2003. Extension, crustal structure and magmatism at the outer Vøring Basin, Norwegian margin, *J. Geol. Soc., Lond.,* **160,** 197–208.

Gernigon, L., Ringenbach, J.C., Planke, S. & Le Gall, B., 2004. Deep structures and breakup along volcanic rifted margins: insights from integrated studies along the outer Vøring Basin (Norway), *Mar. Petrol.Geol.,* **21,** 363–372.

Gudlaugsson, S.T., Gunnarsson, K., Sand, M. & Skogseid, J., 1988. Tectonic and volcanic events at the Jan Mayen Ridge microcontinent, Geological Society, London, Special Publications, **39,** pp. 85–93.

Hamann, N.E., Whittaker, R.C. & Stemmerik, L., 2005. Geological development of the Northeast Greenland Shelf, in *Petroleum Geology: North-West Europe and Global Perspectives-Proceedings of the 6th Petroleum Geology Conference,* pp. 887–902, eds Doré, A.G. & Vining, B.A., Geological Society, London.

Hartz, E., Eide, E.A., Andresen, A., Midbøe, P., Hodges, K.V. & Kristiansen, S.N., 2002. $^{40}Ar/^{39}Ar$ geochronology and structural analysis: basin evolution and detrical feedback mechanisms, Hold with Hope region, East Greenland, *Norwegian J. Geol.,* **82,** 341–358.

Henriksen, N., Higgins, A., Kalsbeek, F. & Pulvertaft, T., 2000. Greenland from Archaean to Quarternary; descriptive text to the geological map of Greenland, 1: 2 500 000, *Geol. Greenland Surv. Bull.,* **185,** 1–93.

Hinz, K., 1981. A hypothesis on terrestrial catastrophes wedges of very thick oceanward dipping layers beneath passive continental margins; their origin and palaeoenvironmental significance, *Geologisches Jahrbuch,* **E2,** 3–28.

Hinz, K., Mutter, J.C., Zehnder, C.M. & Group, N.S., 1987. Symmetric conjugation of continent-ocean boundary structures anlong the Norwegian and East Greenland margins, *Mar. Petrol. Geol.,* **3,** 166–187.

Hinz, K., Eldholm, O., Block, M. & Skogseid, J., 1993. Evolution of North Atlantic volcanic continental margins, in *Perol. Geol. of Northwest Europe: Proceedings of the 4th Conference,* pp. 901–913.

Holbrook, W.S. *et al*., 2001. Mantle thermal structure and active upwelling during continental breakup in the North Atlantic, *Earth planet. Sci. Lett.,* **190,** 251–266.

Hopper, J.R., Dahl-Jensen, T., Holbrook, W.S., Larsen, H.C., Lizarralde, D., Korenaga, J., Kent, G.M. & Kelemen, P.B., 2003. Structure of the SE Greenland margin from seismic reflection and refraction data: implications for nascent spreading center subsidence and asymmetric crustal accretion during North Atlantic opening, *J. geophys. Res.,* **108,** 2269.

Jakobsson, M., Cherkis, N.Z., Woodward, J., Macnab, R. & Coakley, B., 2000. New grid of Arctic bathymetry aids scientists and mapmakers, *EOS Trans. Am. Geophys. Union,* 81, 89, 93, 96.

Jokat, W. *et al*., 2004. Marine geophysics, *Reports on Polar and Marine Research*, **475**, 11–34.

Kelemen, P.B. & Holbrook, W.S., 1995. Origin of thick, high-velocity igneous crust long the U.S. East Coast Margin, *J. geophys. Res.,* **100,** 10077–10094.

King, S.D. & Anderson, D.L., 1995. An alternative mechanism for flood basalt formation, *Earth planet. Sci. Lett.,* **136,** 269–279.

King, S.D. & Anderson, D.L., 1998. Edge-driven convection, *Earth planet. Sci. Lett.,* **160,** 289–296.

Kodaira, S. *et al*., 1995. Crustal structure of the Lofoten continental margin, off N. Norway, by OBS refraction studies, *Geophys. J. Int.,* **121,** 907–924.

Kodaira, S., Mjelde, R., Gunnarson, K., Shiobara, H. & Shimamura, H., 1997. Crustal structure of the Kolbeinsey Ridge, North Atlantic, obtained by use of ocean bottom seismographs, *J. geophys. Res.,* **102,** 3131–3151.

Kodaira, S., Mjelde, R., Gunnarson, K., Shiobara, H. & Shimamura, H., 1998a. Structure of the Jan Mayen microcontinent and implications for its evolution, *Geophys. J. Int.,* **132,** 383–400.

Kodaira, S., Mjelde, R., Gunnarson, K., Shiobara, H. & Shimamura, H., 1998b. Evolution of the oceanic crust on the Kolbeinsey Ridge, north of Iceland, over the past 22 Myr, *Terra Nova,* **10,** 27–31.

Korenaga, J., 2004. Mantle mixing and continental breakup magamtism, *Earth planet. Sci. Lett.,* **218,** 463–473.

Korenaga, J., Holbrook, W.S., Kent, G.M., Kelemen, P.B., Detrick, R.S., Larsen, H.C., Hopper, J.R. & Dahl-Jensen, T., 2000. Crustal structure of the southeast Greenland margin from joint refraction and reflection seismic tomography, *J. geophys. Res.,* **105,** 21 591–21 614.

Korenaga, J., Kelemen, P.B. & Holbrook, W.S., 2002. Methods of resolving the origin of large igneous provinces from crustal seismology, *J. geophys. Res.,* **107,** 2178.

Larsen, H.C., 1990. The East Greenland Shelf, in *The Geology of North America,* pp. 185–210 Geological Society of America, Boulder, Colo.

Larsen, H.C., Saunders, A.D. & Clift, P.D., 1994. *Proc. ODP, Init. Rep., 152 (Pt. 1),* in *Ocean Drilling Program, College Station, TX*.

Lawver, L.A. & Müller, D.R., 1994. Iceland "hotspot" track, *Geology,* **22,** 311–314.

Ludwig, W.J., Nafe, J.E. & Drake, C.L., 1970. Seismic refraction, in *The Sea,* pp. 53–84, ed. Maxwell, A.E., Wiley-Interscience, New York.

Mandler, H. & Jokat, W., 1998. The crustal structure of central east Greenland: results from combined land-sea seismic refraction experiments, *Geophys. J. Int.,* **135,** 63–76.

McKenzie, D. & Bickle, M.J., 1988. The volume and composition of melt generated by extension of the lithosphere, *J. Petrol.,* **29,** 625–679.

Meyer, R., van Wijk, J. & Gernigon, L., 2007. The North Atlantic Igneous Province: a review of the models for its formation, in *Plates, Plumes, and Planetary Processes,* pp. 430 p., eds Foulger, G.R. & Jurdy, D.M., Geological Society of America Special Paper.

Mjelde, R., Kodaira, S., Shimamura, H., Kananzawa, T., Shiobara, H., Berg, E.W. & Riise, O., 1997. Crustal structure of the central part of the Vøring Basin, mid-Norway margin, from ocean bottom seismographs, *Tectonophysics,* **277,** 235–257.

Mjelde, R. *et al*., 1998. Crustal structure of the northern part of the Vøring Basin, mid-Norway margin, from wide-angle seismic and gravity data, *Tectonophysics,* **293,** 175–205.

Mjelde, R. *et al*., 2001. Crustal structure of the outer Vøring Plateau, offshore Norway, from ocean bottom seismic and gravity data, *J. geophys. Res.,* **106,** 6769–6791.

Mjelde, R., Kasahara, J., Shimamura, H., Kamimura, A., Kananzawa, T., Kodaira, S., Raum, T. & Shiobara, H., 2002. Lower crustal velocity-anomalies; magmatic underplating or serpentinized peridotite? Evidence from the Vøring Margin, NE Atlantic, *Mar. Geophys. Res.,* **23,** 169–183.

Mjelde, R., Shimamura, H., Kananzawa, T., Kodaira, S., Raum, T. & Shiobara, H., 2003. Crustal lineaments, distribution of lower crustal intrusives and structural evolution of the Voering Margin, NE Atlantic; new insights from wide-angle seismic models, *Tectonophysics,* **369,** 199–218.

Mjelde, R., Raum, T., Myhren, B., Shimamura, H., Murai, Y., Takanami, T., Karpuz, R. & Naess, U., 2005. Continent-ocean transition on the Voring Plateau, NE Atlantic, derived from densely spaced ocean bottom seismometer data, *J. geophys. Res.,* **110,** B05101, 1–19.

Morgan, W.J., 1971. Convection plumes in the lower mantle, *Nature,* **230,** 42–43.

Morgan, J.V., Barton, P.J. & White, R.S., 1989. The Hatton Bank continental margin—III. Structure from wide-angle OBS and multichannel seismic refraction profiles, *Geophys. J. Int.,* **98,** 367–384.

Mosar, J., Lewis, G. & Torsvik, T.H., 2002b. North Atlantic sea-floor spreading rates: implications for the Tertiary development of inversion structures of the Norwegian-Greenland Sea, *J. Geol. Soc., Lond.,* **159,** 503–515.

Mutter, J.C. & Zehnder, C.M., 1988. Deep crustal and magmatic processes: the inception of seafloor spreading in the Norwegian-Greenland Sea, *Geol. Soc. Spec. Publ. Lond.,* **39,** 35–48.

Mutter, J.C., Buck, W.R. & Zehnder, C.M., 1988. Convective partial melting 1. A model for the firmation of thick basaltic sequences duirng the initiation of spreading, *J. geophys. Res.,* **93,** 1031–1048.

Myhre, A.M. & Thiede, J., 1995. North Atlantic-Arctic Gateways, *Proc. Ocean Drill. Program Initial Rep.,* **151**.

Nafe, J.E. & Drake, C.L., 1957. Variations with depth in shallow and deep water marine sediments of porosity, density and the velocity of compresional and shear waves, *Geophysics,* **22,** 523–552.

Nielsen, T.K. & Hopper, J.R., 2004. From rift to drift: mantle melting during continental breakup, *Geochem. Geophys. Geosyst.,* **5,** 1–24.

Nielsen, T.K., Larsen, H.C. & Hopper, J.R., 2002. Contrasting rifted margin styles south of Greenland: implications for mantle dynamics, *Earth planet. Sci. Lett.,* **200,** 271–286.

Olesen, O. *et al*., 2007. An improved tectonic model for the Eocene opening of the Norwegian-Greenland Sea: use of modern magnetic data, *Mar. Petrol. Geol.,* **24,** 53–66.

Price, S., Brodie, J., Whitham, A. & Kent, R., 1997. Mid-Tertiary rifting and magmatism in the Traill Ø region, East Greenland, *J. geol. Soc. Lond.,* **154,** 419–434.

Raum, T. *et al*., 2002. Crustal structure of the southern part of the Vøring Basin, mid-Norway margin, from wide-angle seismic and gravity data, *Tectonophysics,* **355,** 99–126.

Rowley, D.B. & Lottes, A.L., 1988. Plate-kinematic reconstructions of the North Atlantic and Arctic: late Jurassic to Present, *Tectonophysics,* **155,** 73–120.

Saunders, A.D., Fitton, J.G., Kerr, A.C., Norry, M.J. & Kent, R.W., 1997. The North Atlantic Igneous Province, in *Large Igneous Provinces,* pp. 45–94, eds Mahoney, J.J. & Coffin, M.F., American Geophysical Union Monograph.

Saunders, A.D., Larsen, H.C. & Wise, S.W.J., 1998. *Proceedings of the Ocean drilling Program, Scientific Results*, in *Ocean Drilling Program*, College Station, TX.

Sawyer, D.S., 1985. Total tectonic subsidence: a parameter for distinguishing crust type at the U.S. Atlantic continental margin, *J. geophys. Res.,* **90,** 7751–7769.

Schlindwein, V., 1998. Architecture and evolution of the continental crust of east Greenland from integrated geophysical studies, in Reports on Polar and Marine Research, pp. 1–148, Bremerhaven.

Schlindwein, V. & Jokat, W., 1999. Structure and evolution of the continental crust of northern east Greenland from integrated geophysical studies, *J. Geophys. Res.,* **104,** 15227–15245.

Schlindwein, V. & Jokat, W., 2000. Post-collisional extension of the East Greenland Caledonides: a geophysical perspective, *Geophys. J. Int.,* **140,** 559–567.

Schmidt-Aursch, M.C. & Jokat, W., 2005a. The crustal structure of central East Greenland-I: from the Caledonian orogen to the Tertiary igneous province, *Geophys. J. Int.,* **160,** 736–752.

Schmidt-Aursch, M.C. & Jokat, W., 2005b. The crustal structure of central East Greenland-II: from the Precambrian shield to the recent mid-oceanic ridges, *Geophys. J. Int.,* **160,** 753–760.

Skogseid, J., Planke, S., Faleide, J.I., Pedersen, T., Eldholm, O. & Neverdal, F., 2000. NE Atlantic continental rifting and volcanic margin formation, in *Dynamics of the Norwegian Margin,* pp. 295–326, ed. Nøttvedt, A., Geological Society Special Publication, London.

Sleep, N.H., 1996. Lateral flow of hot plume material ponded at sublithospheric depths, *J. Geophys. Res.,* **101,** 28 065–28 083.

Smith, W.H.F. & Wessel, P., 1990. Gridding with continuous curvature splines in tension, *Geophysics,* **55,** 293–305.

Surlyk, F., 1990. Timing, style and sedimentary evolution of Late Palaeozoic-Mesozoic extensional basins of East Greenland, in *Tectonic Events Responsible for Britain's Oil and Gas Reserves,* pp. 107–125, eds Hardman, R.F.P. & Brooks, J., Geol. Soc. Spec. Publ.

Tsikalas, F., Faleide, J.I. & Eldholm, O., 2001. Lateral variations in tectono-magmatic style along the Lofoten-Verstålen volcanic margin off Norway, *Mar. Petrol. Geol.,* **18,** 801–832.

Tsikalas, F., Eldholm, O. & Faleide, J.I., 2002. Early Eocene sea floor spreading and continent-ocean boundary between Jan Mayen and Senja fracture zones in the Norwegian-Greenland Sea, *Mar. Geophys. Res.,* **23,** 247–270.

Tsikalas, F., Eldholm, O. & Faleide, J.I., 2005. Crustal structure of the Lofoten-Vesterålen continental margin, off Norway, *Tectonophysics,* **404,** 151–174.

Upton, B.G.J., Emeleus, C.H., Rex, D.C. & Thirlwall, M.F., 1995. Early Tertiary magmatism in northeast Greenland, *J. geol. Soc. Lond.n,* **152,** 959–964.

van Wijk, J.W., Huismans, R.S., Ter Vorrde, M. & Cloetingh, S.A.P.L., 2001. Melt generation at volcanic continental margins: no need for a mantle plume? *Geophys. Res. Lett.,* **28,** 3995–3998.

Verhoef, J., Macnab, W.R., Arkani-Hamed, R. & Team, J.M.o.t.P., 1996. Magnetic anomalies of the Arctic and North Atlantic Oceans and adjacent land areas; Open File 3125, *Geological Survey of Canada*.

Voss, M. & Jokat, W., 2007. Continent–ocean transition and voluminous magmatic underplating derived from P-wave velocity modelling of the East Greenland continental margin, *Geophys. J. Int.,* **170,** 580–604.

Watt, S.W., 1994. Stratigraphy and correlation of the tertiary plateau basalts in North-East Greenland, *Rapp. Grønlands geol. Unders.,* **162,** 195–200.

Weigel, W. *et al*., 1995. Investigations of the east Greenland continental margin between 70° and 72°N by deep seismic sounding and gravity studies, *Mar. Geophys. Res.,* **17,** 167–199.

Wessel, P. & Smith, W.H.F., 1998. New, improved version of generic mapping Tools released, *EOS Trans. Am. Geophys. Union,* **79,** pp. 579.

White, R.S., 1992. Magmatism during and after continental break-up, in *Magmatism and the Causes of Continental Break-up,* pp. 1–16, eds Storey, B.C., Alabaster, T. & Pankhurst, R.J., Geological Society Special Publication.

White, R. & McKenzie, D., 1989. Magmatism at rift zones: the generation of volcanic continental margins and flood basalts, *J. geophys. Res.,* **94,** 7685–7729.

White, R.S., Spence, G.D., Fowler, S.R., McKenzie, D., Westbrook, G.K. & Bowen, A.N., 1987. Magmatism at rifted continental margins, *Nature,* **330,** 439–444.

White, R.S., McKenzie, D. & O'Nions, R.K., 1992. Oceanic crustal thickness from seismic measurements and rare earth element inversions, *J. geophys. Res.,* **97,** 19683–19715.

Whitmarsh, R.B. & Miles, P.R., 1995. Models of the development of the West Iberia rifted continental margin at 40°30'N deduced from surface and deep-tow magnetic anomalies, *J. geophys. Res.,* **100,** 3789–3806.

Whitmarsh, R.B., White, R.S., Horsefield, S.J., Sibuet, J.C., Recq, M. & Louvel, V., 1996. The ocean-continent boundary off the western continental margin of Iberia; crustal structure of Galicia Bank, *J. geophys. Res.,* **101**.

Zelt, C.A. & Smith, R.B., 1992. Seismic traveltime inversion for 2-D crustal velocity structure, *Geophys. J. Int.,* **108,** 16–34.